Hepatitis C virus is a major cause of chronic liver diseases, such as hepatitis, cirrhosis, and hepatocellular carcinoma, with substantial morbidity and mortality (3, 4). The prevalence of HCV is about 2%, representing 120 million people worldwide. Current standard treatment using pegylated interferon and ribavirin is effective in only half the patients infected with HCV genotype 1, which is the most resistant of all HCV genotypes to interferon-based therapy. Therefore, development of complementary and/or alternative drugs for treatment of HCV infection is still needed from both clinical and economic points of view. In this regard, antiviral substances obtained from medicinal plants are potentially good targets to study (5–7), as has also been reported for other viruses (8).

Morinda citrifolia belongs to the Rubiaceae family and is thought to have originated in Indonesia. This common plant is distributed widely in the Indo-Pacific region. The fruits and leaves of *M. citrifolia* are food sources for local people and are also used as a treatment for infections and inflammatory diseases (9) in traditional medicine. Nowadays, the juice from the ripe fruits, traditionally known as "noni," is sold as a health food even in industrialized countries. It has been reported that methanol or ethanol extracts of *M. citrifolia* fruits and/or leaves have antibacterial activities against some bacteria, such as *Staphylococcus aureus* (10) and *Mycobacterium tuberculosis* (11). Using an HCV subgenomic replicon, anti-HCV activity has also been reported for both methanol and ethanol extracts of *M. citrifolia* fruits (12). In this study, we used an HCV infection system in cultured cells to explore the anti-HCV activities of methanol extracts of the fruits (ripe and frozen), leaves, roots, and branches of *M. citrifolia*. We report here that a methanol extract of *M. citrifolia* leaves and its subfractions, as well as an isolated compound, pheophorbide a, and its catabolite, pyropheophorbide a, possess antiviral activities against HCV.

MATERIALS AND METHODS

Cells and viruses

Huh7.5 cells and the plasmid pFL-J6/JFH1 to produce the J6/JFH1 strain of HCV genotype 2a (13) were kindly provided by Dr. C.M. Rice (Rockefeller University, New York, NY, USA). The J6/JFH1-P47 strain of HCV was prepared as described previously (14). Huh7.5 cells were cultured in Dulbecco's modified Eagle's medium (Wako, Osaka, Japan) supplemented with FBS (Biowest, Nuaillé, France), non-essential amino acids (Invitrogen, Carlsbad, CA, USA), penicillin (100 IU/mL), and streptomycin (100 μg/mL) (Invitrogen) at 37 °C in a 5% CO_2 incubator.

Extraction of various parts of *M. citrifolia* and further fractionation and purification of the samples

M. citrifolia fruits (ripe and frozen), leaves, roots, and branches were collected in Okinawa Prefecture, Japan. Methanol extracts of each of these components of *M. citrifolia* were prepared and subjected to purification procedures, as described previously (15–18). In brief, the plant components were dried at room temperature, pulverized according to their characteristics, and then extracted with methanol at 50 °C for 6 hr. The extracts were then filtered and the filtrates concentrated by using an evaporator at temperatures not exceeding 40 °C. The residues thus obtained were resuspended in water and successively partitioned between *n*-hexane, ethyl acetate, and 1-butanol. Next, the *n*-hexane extracts were subjected to recycling preparative HPLC (solvent system, 100% methanol; column, GS-320; ID, 21.5 mm × 500 mm; flow rate, 5.0 mL/min; detection, UV 210 nm) to yield five fractions (Fr. 1–5). Fr. 5 was subjected to HPLC separation (solvent system, 100% methanol; column, TSK-gel GOLIGOPW [Tosoh Bioscience Diagnostics, Tessenderlo, Belgium]; ID, 4.6 mm × 250 mm; flow rate, 1.0 mL/min; detection, UV 210 nm) to yield three fractions (Fr. 5-1 to 5-3). Fr. 5-1 was rechromatographed by ODS column chromatography (Varian Mega Bond-Elut C18; Agilent Technologies Japan, Tokyo, Japan) with 100% methanol as an eluent to yield three fractions (Fr. 5-1-1 to 5-1-3). Fr. 5-1-3 was subjected to HPLC (solvent system, methanol–acetone [9:1]; column, Cosmosil Cholester [Nacalai Tesque, Kyoto, Japan]; ID, 4.6 mm × 450 mm; flow rate, 2 mL/min; detection, UV 400 nm) to obtain two fractions (Fr. 5-1-3-1 and 5-1-3-2).

The ^{1}H-NMR spectra were measured with a JEOL ECA 500 spectrometer (500 MHz; Tokyo, Japan). HPLC was performed on a JASCO LC-2000 plus system (JASCO, Tokyo, Japan). A Merck TLC plate (Art. 5715; Merck, Darmstadt, Germany) was used for TLC comparisons.

Chemicals

Chlorophyll a (from spinach) and sodium copper chlorophyllin were purchased from Sigma–Aldrich (St Louis, MO, USA) and pheophytin a from Wako Pure Chemical Industries (Osaka, Japan). Pheophorbide a and pyropheophorbide a were purchased from Frontier Scientific (Logan, UT, USA).

Analysis of anti-HCV activities of plant extracts and purified compounds

For anti-HCV activity assay, test samples were weighed and dissolved in DMSO to obtain stock solutions, which were stored at −20 °C until used. Huh7.5 cells were

seeded in 24-well plates (1.9×10^5 cells/well). A fixed amount of HCV was mixed with serial dilutions of the plant extracts (100, 30, 10, 3, and 1 μg/mL) and inoculated into the cells. After 2 hr, the cells were washed with medium to remove the residual virus and further incubated in medium containing the same concentrations of the plant extracts as those used during virus inoculation. In order to assess the mode of action of the samples examined, in some experiments treatment with the plant extracts was performed only during virus inoculation or only after virus inoculation until virus harvest. Culture supernatants were obtained at 1 and 2 days post-infection and titrated for virus infectivity, as described previously (19). Virus and cells treated with medium containing 0.1% DMSO served as controls. Percent inhibition of virus infectivity by the samples was calculated by comparing with the controls; IC_{50} were determined.

Time-of-addition experiments

To determine whether anti-HCV activities of the test samples occurred at the entry or the post-entry step, time-of-addition experiments were performed as described previously (6, 7). In brief:

1 HCV was mixed with each of the compounds and the mixture was inoculated into the cells. After virus adsorption for 2 hr, the residual virus and test sample were removed and the cells refed with fresh medium without the test sample for 46 hr. This experiment examines antiviral effect during the entry step.

2 HCV was inoculated into the cells in the absence of test samples. After virus adsorption for 2 hr, the residual virus was removed and the cells refed with fresh medium containing the test samples for 46 hr. This experiment examines the antiviral effect during the post-entry step.

3 As a positive control, HCV mixed with the test sample was inoculated into the cells. After virus adsorption for 2 hr, the residual virus and test sample were removed and the cells refed with fresh medium containing the test samples for 46 hr.

WST-1 assay for cytotoxicity

WST-1 assay was performed as described previously with a slight modification (19). In brief, Huh7.5 cells in 96-well plates were treated with serial dilutions of the plant extracts or 0.1% DMSO as a control for 48 hr. After this treatment, 10 μL of WST-1 reagent (Roche, Mannheim, Germany) was added to each well and the cells cultured for 4 hr. The WST-1 reagent is absorbed by the cells and converted to formazan by mitochondrial dehydrogenases. The amount of formazan, which correlates with the number of living cells, was determined by measuring the absorbance of each well using a microplate reader at 450 and 630 nm. Percent cell viability compared to the control was calculated for each dilution of the plant extracts and CC_{50} were determined.

Immunoblotting

Immunoblotting analysis was performed as described previously (6, 7, 20). In brief, cells lysed with an SDS sample buffer were subjected to SDS-PAGE and transferred onto polyvinylidene difluoride membranes (Millipore, Bedford, MA, USA). The membranes were incubated with the respective primary antibody, such as mouse monoclonal antibodies against HCV NS3 and GAPDH (Millipore). Horseradish peroxidase-conjugated goat anti-mouse immunoglobulin (Invitrogen) was used to visualize the respective proteins by means of an enhanced chemiluminescence detection system (GE Healthcare, Buckinghamshire, UK).

Real-time quantitative RT-PCR

Real-time quantitative RT-PCR was performed as described previously (6, 7, 20). In brief, 1 μg of total RNA extracted from the cells using a ReliaPrep RNA cell miniprep system (Promega, Madison, WI, USA) was reverse transcribed using a GoScript Reverse Transcription system (Promega) with random primers. The resultant cDNA was subjected to real-time quantitative PCR analysis using SYBR Premix Ex Taq (TaKaRa, Kyoto, Japan) in a MicroAmp 96-well reaction plate and an ABI PRISM 7500 system (Applied Biosystems, Foster City, CA, USA). The HCV NS5A-specific primers used were 5′-AGACGTATTGAGGTCCATGC-3′ (sense) and 5′-CCGCAGCGACGGTGCTGATAG-3′ (antisense). Human GAPDH gene expression measured by using primers 5′-GCCATCAATGACCCCTTCATT-3′ (sense) and 5′-TCTCGCTCCTGGAAGATGG-3′ (antisense) served as internal controls.

Statistical analysis

Results are expressed as mean ± SEM. Statistical significance was evaluated by Student's *t*-test. $P < 0.05$ was considered statistically significant.

RESULTS

Anti-HCV activities of methanol extracts of *M. citrifolia* fruits, leaves, roots, and branches

Methanol extracts of the fruits (ripe and frozen), leaves, roots, and branches of *M. citrifolia* were examined for antiviral activities against the HCV J6/JFH1-P47 strain.

It was found that a methanol extract of *M. citrifolia* leaves at a concentration of 30 μg/mL inhibits HCV infection by 98.3%, whereas extracts of ripe fruits, frozen fruits, roots and branches at the same concentration inhibit HCV infection by 23.4%, 34.0%, 59.6%, and 27.7%, respectively. The following analyses, therefore, focus on the extract from *M. citrifolia* leaves.

Anti-HCV activities of further purified samples of *M. citrifolia* leaves

The methanol extract of *M. citrifolia* leaves was further partitioned with different solvents, comprising *n*-hexane, ethyl acetate, 1-butanol and water, and their IC_{50}, CC_{50}, and SIs (SI: CC_{50}/IC_{50}) determined. The IC_{50} values of the partitions with *n*-hexane and ethyl acetate were 6.1 and 6.6 μg/mL, respectively; both of these showed stronger anti-HCV activities than did the methanol extract, which had an IC_{50} of 20.6 μg/mL (Table 1). The *n*-hexane-partitioned sample was fractionated into a further five fractions by a recycling preparative HPLC method; of these fractions, only Fr. 5 showed anti-HCV activity, the IC_{50} being 7.8 μg/mL (Table 2). Fr. 5 was therefore further purified by HPLC, ODS column chromatography and another HPLC and Fr. 5-1-3-2 identified as the most potent and purified fraction, having an IC_{50} of 4.6 μg/mL.

On TLC analysis (detection: UV irradiation 366 nm) of Fr. 5-1-3-2, a red-fluorescent spot was detected, suggesting that Fr. 5-1-3-2 consists almost solely of chlorophyll a and its degraded products. The presence of pheophorbide a, which is reportedly the major catabolite of chlorophyll a (21, 22), was confirmed by direct comparison with a standard sample by TLC analysis. Structural analyses using HPLC and NMR identified the purified compound as pheophorbide a (23).

Anti-HCV activities of pheophorbide a and pyropheophorbide a

Pheophorbide a is a breakdown product of chlorophyll. In its breakdown process, chlorophyll loses the Mg^{2+} ion through demetallation to generate pheophytin a in senescent leaves (21, 22). Pheophytin a is catabolized to pheophorbide a through dephytylation. In fruits, dephytylation of chlorophyll takes place first to generate chlorophyllide, which is then catabolized to pheophorbide a through demetallation. Pheophorbide a is further catabolized to generate pyropheophorbide a. On the other hand, sodium copper chlorophyllin is a semi-synthetic compound in which the Cu^{2+} ion replaces the Mg^{2+} ion.

Anti-HCV activities of commercially available, reagent-grade chlorophyll a and its-related compounds were examined. It was found that chlorophyll a barely, and sodium copper chlorophyllin and pheophytin a only weakly, exhibit anti-HCV activities (IC_{50} = 220, 32.0, and 54.5 μg/mL, respectively). On the other hand, pheophorbide a and pyropheophorbide a showed potent anti-HCV activities with IC_{50} of 0.3 and 0.2 μg/mL, respectively (Table 3).

Table 1. Anti-HCV activity (IC_{50}), cytotoxicity (CC_{50}) and selectivity index (SI) of a methanol extract and solvent partitions obtained from of *M. citrifolia* leaves

Sample	IC_{50} (μg/mL)	CC_{50} (μg/mL)	SI
Methanol extract	20.6	>30‡	>1.5
n-Hexane partition	6.1	>30‡	>4.9
Ethyl acetate partition	6.6	>30‡	>4.5
n-Butanol partition	20.8	>30‡	>1.5
Water partition	>30†	>30‡	na

†no detectable HCV inhibition at 30 μg/mL. ‡no detectable cytotoxicity at 30 μg/mL; na, not applicable.

Table 2. Anti-HCV activity (IC_{50}), cytotoxicity (CC_{50}), and selectivity index (SI) of fractions from *M. citrifolia* leaves obtained by recycling preparative HPLC and ODS column chromatography

Sample	IC_{50} (μg/mL)	CC_{50} (μg/mL)	SI
Fr. 1	>30	>30‡	na
Fr. 2	>30	>30‡	na
Fr. 3	>30†	>30‡	na
Fr. 4	>30†	>30‡	na
Fr. 5	7.8	>30‡	>3.8
ODS column chromatography			
Fr. 5-1-1	8.6	>30‡	>3.5
Fr. 5-1-2	5.2	>30‡	>5.8
Fr. 5-1-3	4.6	>30‡	>6.5
HPLC			
Fr. 5-1-3-1	>30	>30	na
Fr. 5-1-3-2	4.6	>30	>6.5

†no detectable HCV inhibition at 30 μg/mL. ‡no detectable cytotoxicity at 30 μg/mL; na, not applicable.

Table 3. Anti-HCV activity (IC_{50}), cytotoxicity (CC_{50}), and selectivity index (SI) of commercially available chlorophyll a, sodium copper chlorophyllin, pheophytin a, pheophorbide a, and pyropheophorbide a

Sample	IC_{50} (μg/mL)	CC_{50} (μg/mL)	SI
Chlorophyll a	220	>300	na
Sodium copper chlorophyllin	32.0	158	4.9
Pheophytin a	54.5	328	6.0
Pheophorbide a	0.3	10.0	33
Pyropheoborbide a	0.2	7.2	36

na, not applicable.

Table 4. Time-of-addition analysis of pheophorbide a and pyropheophorbide a against HCV

Compound (μg/mL)	Anti-HCV activity†		
	During virus inoculation	After virus inoculation	During & after virus inoculation
Pheophorbide a (1.0)	64.0	95.3	98.7
Pyropheophorbide a (0.5)	53.0	98.1	99.7

†% inhibition when tested by time-of-addition analysis.

Mode-of-action of pheophorbide a and pyropheophorbide a

To determine whether the anti-HCV effects of pheophorbide a and pyropheophorbide a are exerted during the entry or post-entry step, time-of-addition experiments were performed. It was found that, when added to the culture only during virus adsorption followed by virus entry, pheophorbide a (1.0 μg/mL) and pyropheophorbide a (0.5 μg/mL) inhibit HCV infection by 64.0% and 53.0%, respectively (Table 4). On the other hand, when added to the culture only after virus inoculation, they inhibited HCV replication by 95.3% and 98.1%, respectively. These results suggest that pheophorbide a and pyropheophorbide a act during both the entry and post-entry steps.

Inhibition of HCV RNA replication and HCV protein synthesis by pheophorbide a and pyropheophorbide a

To further confirm that pheophorbide a and pyropheophorbide a exert their anti-HCV activities not only during the virus entry step but also during the post-entry step (after the virus has entered the cells), Huh7.5 cells were inoculated with HCV for 2 hr in the absence of the test samples, and then treated with either one of the compounds for 1–2 days. Real-time quantitative RT-PCR and immunoblotting analyses demonstrated that both pheophorbide a and pyropheophorbide a inhibit HCV RNA replication in a dose-dependent manner (Fig. 1a) and, consequently, inhibit HCV protein synthesis in the cells (Fig. 1b).

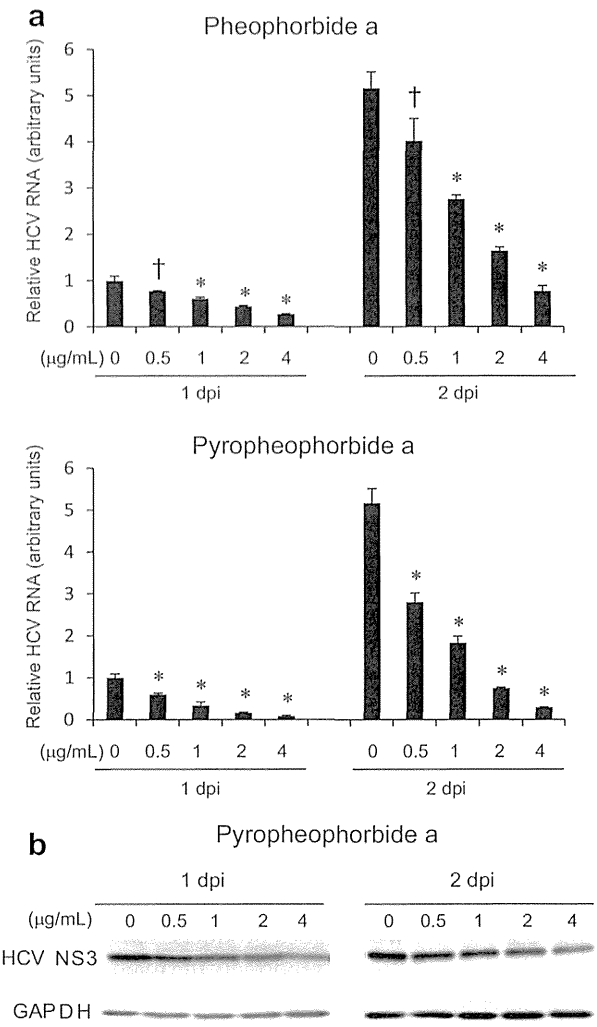

Fig. 1. Effects of pheophorbide a and pyropheophorbide a on HCV RNA replication and protein synthesis. (a) Huh 7.5 cells were inoculated with HCV J6/JFH1 at an MOI of 2.0. After 2 hr, the cells were washed with medium to remove residual virus and treated with either pheophorbide a or pyropheophorbide a (both at 0.5, 1.0, 2.0, and 4 μg/mL) or left untreated, and then subjected to real-time quantitative RT-PCR analysis 1 and 2 dpi. The HCV RNA amounts in the cells are normalized to degree of GAPDH mRNA expression. Data represent means ± SEMs of data from two independent experiments. The value for the untreated control at 1 dpi is arbitrarily expressed as 1.0. *, $P < 0.0001$. (b) Amounts of the HCV NS3 protein in the pyropheophorbide a-treated cells described in (a) were measured by western blot analysis using monoclonal antibody against the NS3 protein. GAPDH served as an internal control to verify equal amounts of sample loading.

DISCUSSION

It has been reported that methanol and ethanol extracts of *M. citrifolia* fruits show anti-HCV activities in a HCV subgenomic replicon system (12). In the present study, we found that a methanol extract of *M. citrifolia* leaves inhibits HCV replication in an HCV cell culture system more efficiently than do *M. citrifolia* fruits extracts (98% vs. ca. 30% inhibition at 30 μg/mL), the IC_{50} of the *M. citrifolia* leaves extract being 20.6 μg/mL (Table 1). Subsequent bioactivity-guided purification and structural analysis demonstrated that pheophorbide a, known to be the major catabolite of chlorophyll a (21, 22), and

its related catabolite, pyropheophorbide a, have potent anti-HCV activities (Table 3). A time-of-addition study suggested that pheophorbide a and pyropheophorbide a act during both the entry and post-entry steps (Table 4). It should be noted that, although Fr. 5-1-3-2 purified from the *M. citrifolia* leaves extract consists almost entirely of pheophorbide a, its anti-HCV activity is much weaker than that of reagent-grade pheophorbide a (Tables 2, 3). One possible explanation for this apparent discrepancy is that a copurified small molecule(s) in the fraction interfered with the anti-HCV activity of pheophorbide a. Further studies are needed to clarify this issue.

Pheophorbide a reportedly inhibits influenza A virus infection (24). Pheophorbide a and pyropheophorbide a also reportedly show antiviral activities against herpes simplex virus type 2 and influenza A virus, but not poliovirus (25). Given that herpes simplex virus type 2 and influenza A virus are envelope viruses whereas poliovirus is a non-envelope virus, Bouslama *et al.* speculate that pheophorbide a and pyropheophorbide a inhibit envelope viruses, targeting specific envelope proteins and thereby interfering with viral binding to the host cell receptors (25). On the other hand, our present results suggest that pheophorbide a and pyropheophorbide a inhibit HCV infection not only during the viral binding/entry step but also during the post-entry step (Table 4, Fig. 1). The post-entry step can be further divided into the following stages of the HCV lifecycle: (i) uncoating of the viral particles and capsid; (ii) synthesis and processing of the viral proteins and replication of the viral genome; and (iii) assembly, intracellular transport, and release of the viral particles (1, 26, 27). Now that we have shown that pheophorbide a and pyropheophorbide a inhibit HCV infection during the post-entry step, it is important to elucidate the specific molecular mechanism(s) in the viral lifecycle targeted by those compounds.

Pheophorbide a and pyropheophorbide a are known to induce photosensitivity: the resultant photo-activated characteristics play important anti-tumor roles in photodynamic therapy using pheophorbide a and its derivatives (28–30). Pheophorbide a also reportedly induces apoptosis of cancer cells and potentiates immunostimulating functions of macrophages (31, 32). However, photosensitivity can cause serious adverse effects when these agents are used to treat cancer and viral infections. Importantly, the photosensitizing effect can be separated from anti-tumor effect (28). It is therefore tempting to speculate that a new derivative(s) with more potent anti-HCV activities and less capacity to induce photosensitivity could be synthesized from the seed compounds of pheophorbide a and pyropheophorbide a.

It has previously been reported that pheophytin a shows anti-HCV activities with IC_{50} of 4.97 μM (equivalent to 4.3 μg/mL) (33). Also chlorophyllin, a semi-synthetic derivative of chlorophyll, reportedly has antiviral activities against poliovirus and bovine herpesvirus, with IC_{50} of 19.8 and 8.6 μg/mL, respectively (34). However, in our study, compared with the more potent anti-HCV activities of pheophorbide a and pyropheophorbide a, pheophytin a and sodium copper chlorophyllin exhibited only marginal anti-HCV activity, the IC_{50} being 54.5 and 32.0 μg/mL, respectively (Table 3).

In this study, we demonstrated anti-HCV activities of pheophorbide a and pyropheophorbide a using the J6/JFH1 strain of HCV genotype 2a (13, 14). Whether these compounds inhibit replication of other HCV strains of different genotypes is an important question to answer. Currently, some other HCV genotypes, such as genotypes 1a, 1b and 3a to 7a, are available for drug screening tests (2, 35). Such *in vitro* cell culture systems would help in determining the possible anti-HCV activities of pheophorbide a and pyropheophorbide a against different genotypes of HCV.

In conclusion, we have demonstrated that a methanol extract of *M. citrifolia* leaves and certain chlorophyll-derived compounds, such as pheophorbide a and pyropheophorbide a, possess anti-HCV activities. These compounds would be good candidates for seed compounds for developing novel antivirals against HCV.

ACKNOWLEDGMENTS

The authors are grateful to Dr. C.M. Rice (Rockefeller University, New York, NY, USA) for providing Huh-7.5 cells and pFL-J6/JFH1. This study was supported in part by Science and Technology Research Partnerships for Sustainable Development from JST and JICA. It was also performed as part of Japan Initiative for Global Research Network on Infectious Diseases (J-GRID), Ministry of Education, Culture, Sports, Science and Technology, Japan.

DISCLOSURE

The authors have no conflicts of interest to declare.

REFERENCES

1. Moradpour D., Penin F., Rice C.M. (2007) Replication of hepatitis C virus. *Nat Rev Microbiol* **5**: 453–6.
2. Gottwein J.M., Scheel T.K., Jensen T.B., Lademann J.B., Prentoe J.C., Knudsen M.L., Hoegh A.M., Bukh J., Development and characterization of hepatitis C virus genotype 1-7 cell culture systems: role of CD81 and scavenger receptor class B type I and effect of antiviral drugs. *Hepatology* **49** 2009; 364–77.

3. Shepard C.W., Finelli L., Alter M.J. (2005) Global epidemiology of hepatitis C virus infections. *Lancet Infect Dis* **5**: 558–67.
4. Arzumanyan A., Reis H.M., Feitelson M.A. (2013) Pathogenic mechanisms in HBV- and HCV-associated hepatocellular carcinoma. *Nat Rev Cancer* **13**: 123–35.
5. Calland N., Dubuisson J., Rouille Y., Seron K. (2012) Hepatitis C virus and natural compounds: a new antiviral approach?. *Viruses* **4**: 2197–217.
6. Wahyuni T.S., Tumewu L., Permanasari A.A., Apriani E., Adianti M., Rahman A., Widyawaruyanti A., Lusida M.I., Fuad A., Soetjipto D., Nasronudin D., Fuchino H., Kawahara N., Shoji I., Deng L., Aoki C., Hotta H. (2013) Antiviral activities of Indonesian medicinal plants in the East Java region against hepatitis C virus. *Virol J* **10**: 259.
7. Adianti M., Aoki C., Komoto M., Deng L., Shoji I., Wahyuni T.S., Lucida M.I., Soetjipto, Fuchino H., Kawahara N., Hotta H. (2014) Anti-hepatitis C virus compounds obtained from *Glycyrrhiza uralensis* and other *Glycyrrhiza* species. *Microbiol Immunol*. doi: 10.1111/1348-0421.12127. [Epub ahead of print].
8. Ikuta K., Hashimoto K., Kaneko H., Mori S., Ohashi K., Suzutani T. (2012) Anti-viral and anti-bacterial activities of an extract of blackcurrants (*Ribes nigrum L.*). *Microbiol Immunol* **56**: 805–9.
9. Serafini M.R., Santos R.C., Guimarães A.G., Dos Santos J.P., da Conceicão Santos A.D., Alves I.A., Gelain D.P., de Lima Nogueira P.C., Quintans-Júnior L.J., Bonjardim L.R., de Souza Araújo A.A. (2011) *Morinda citrifolia* Linn leaf extract possesses antioxidant activities and reduces nociceptive behavior and leukocyte migration. *J Med Food* **14**: 1159–66.
10. Nakanishi K., Sasaki S., Kiang A.K., Goh J., Kakisawa H., Ohashi M., Goto M., Watanabe J., Yokotani H., Matsumura C., Togashi M. (1965) Phytochemical survey of Malaysian plants preliminary chemical and pharmacological screening. *Chem Pharm Bull* **13**: 882–90.
11. Saludes J.P., Garson M.J., Franzblau S.G., Aguinaldo A.M. (2002) Antitubercular constituents from the hexane fraction of *Morinda citrifolia* Linn. (Rubiaceae). *Phytother Res* **16**: 683–5.
12. Selvam P., Murugesh N., Witvrouw M., Keyaerts E., Neyts J. (2009) Studies of antiviral activity and cytotoxicity of *Wrightia tinctoria* and *Morinda citrifolia*. *Indian J Pharm Sci* **71**: 670–2.
13. Lindenbach B.D., Evans M.J., Syder A.J., Wolk B., Tellinghuisen T.L., Liu C.C., Maruyama T., Hynes R.O., Burton D.R., McKeating J.A., Rice C.M. (2005) Complete replication of hepatitis C virus in cell culture. *Science* **309**: 623–6.
14. Bungyoku Y., Shoji I., Makine T., Adachi T., Hayashida K., Nagano-Fujii M., Ide Y., Deng L., Hotta H. (2009) Efficient production of infectious hepatitis C virus with adaptive mutations in cultured hepatoma cells. *J Gen Virol* **90**: 1681–91.
15. Li S.Y., Fuchino H., Kawahara N., Sekita S., Satake M. (2002) New phenolic constituents from *Smilax bracteata*. *J Nat Prod* **65**: 262–6.
16. Fuchino H., Sekita S., Mori M., Kawahara N., Satake M., Kiuchi F. (2008) A new leishmanicidal saponin from *Brunfelsia grandiflora*. *Chem Pharm Bull* **56**: 93–6.
17. Fuchino H., Kawano M., Mori-Yasumoto K., Sekita S., Satake M., Ishikawa T., Kiuchi F., Kawahara N. (2010) *In vitro* leishmanicidal activity of benzophenanthridine alkaloids from *Bocconia pearcei* and related compounds. *Chem Pharm Bull* **58**: 1047–50.
18. Fuchino H., Daikonya A., Kumagai T., Goda Y., Takahashi Y., Kawahara N. (2013) Two new labdane diterpenes from fresh leaves of Leonurus japonicas and their degradation during drying. *Chem Pharm Bull* **61**: 497–503.
19. Deng L., Adachi T., Kitayama K., Bungyoku Y., Kitazawa S., Ishido S., Shoji I., Hotta H. (2008) Hepatitis C virus infection induces apoptosis through a Bax-triggered, mitochondrion-mediated, caspase 3-dependent pathway. *J Virol* **82**: 10375–85.
20. Deng L., Shoji I., Ogawa W., Kaneda S., Soga T., Jiang D.P., Ide Y.H., Hotta H. (2011) Hepatitis C virus infection promotes hepatic gluconeogenesis through an NS5A-mediated, FoxO1-dependent pathway. *J Virol* **85**: 8556–68.
21. Hörtensteiner S., Kräutler B. (2011) Chlorophyll breakdown in higher plants. *Biochim Biophys Acta* **1807**: 977–88.
22. Hörtensteiner S. (2013) Update on the biochemistry of chlorophyll breakdown. *Plant Mol Biol* **82**: 505–17.
23. Cheng H.H., Wang H.K., Ito J., Bastow K.F., Tachibana Y., Nakanishi Y., Xu Z., Luo T.Y., Lee K.H. (2001) Cytotoxic pheophorbide-related compounds from *Clerodendrum calamitosum* and *C. cyrtophyllum*. *J Nat Prod* **64**: 915–9.
24. Yasuda T., Yamaki M., Iimura A., Shimotai Y., Shimizu K., Noshita T., Funayama S. (2010) Anti-influenza virus principles from *Muehlenbeckia hastulata*. *J Nat Med* **64**: 206–11.
25. Bouslama L., Hayashi K., Lee J.B., Ghorbel A., Hayashi T. (2011) Potent virucidal effect of pheophorbide a and pyropheophorbide a on enveloped viruses. *J Nat Med* **65**: 229–33.
26. Ploss A., Dubuisson J. (2012) New advances in the molecular biology of hepatitis C virus infection: towards the identification of new treatment targets. *Gut* **61** (Suppl 1): i25–35.
27. Aly H.H., Shimotohno K., Hijikata M., Seya T. (2012) In vitro models for analysis of the hepatitis C virus life cycle. *Microbiol Immunol* **56**: 1–9.
28. Nakamura Y., Murakami A., Koshimizu K., Ohigashi H. (1996) Identification of pheophorbide a and its related compounds as possible anti-tumor promoters in the leaves of *Neptunia oleracea*. *Biosci Biotechnol Biochem* **60**: 1028–30.
29. Gil M., Bieniasz M., Seshadri M., Fisher D., Ciesielski M.J., Chen Y., Pandey R.K., Kozbor D. (2011) Photodynamic therapy augments the efficacy of oncolytic vaccinia virus against primary and metastatic tumours in mice. *Br J Cancer* **105**: 1512–21.
30. Rapozzi V., Zorzet S., Zacchigna M., Drioli S., Xodo L.E. (2013) The PDT activity of free and pegylated pheophorbide a against an amelanotic melanoma transplanted in C57/BL6 mice. *Invest New Drugs* **31**: 192–9.
31. Bui-Xuan N.H., Tang P.M., Wong C.K., Fung K.P. (2010) Photo-activated pheophorbide-a, an active component of *Scutellaria barbata*, enhances apoptosis via the suppression of ERK-mediated autophagy in the estrogen receptor-negative human breast adenocarcinoma cells MDA-MB-231. *J Ethnopharmacol* **131**: 95–103.
32. Bui-Xuan N.H., Tang P.M., Wong C.K., Chan J.Y., Cheung K.K., Jiang J.L., Fung K.P. (2011) Pheophorbide a: a photosensitizer with immunostimulating activities on mouse macrophage RAW 264. 7 cells in the absence of irradiation. *Cell Immunol* **269**: 60–7.
33. Wang S.Y., Tseng C.P., Tsai K.C., Lin C.F., Wen C.Y., Tsay H.S., Sakamoto N., Tseng C.H., Cheng J.C. (2009) Bioactivity-guided screening identifies pheophytin a as a potent anti-hepatitis C virus compound from *Lonicera hypoglauca* Miq. *Biochem Biophys Res Commun* **385**: 230–5.
34. Benati F.J., Lauretti F., Faccin L.C., Nodari B., Ferri D.V., Mantovani M.S., Linhares R.E., Nozawa C. (2009) Effects of chlorophyllin on replication of poliovirus and bovine herpesvirus in vitro. *Lett Appl Microbiol* **49**: 791–5.
35. Date T., Morikawa K., Tanaka Y., Tanaka-Kaneko K., Sata T., Mizokami M., Wakita T. (2012) Replication and infectivity of a novel genotype 1b hepatitis C virus clone. *Microbiol Immunol* **56**: 308–17.

Microbiology and Immunology

Microbiol Immunol 2014; 58: 180–187
doi: 10.1111/1348-0421.12127

ORIGINAL ARTICLE

Anti-hepatitis C virus compounds obtained from *Glycyrrhiza uralensis* and other *Glycyrrhiza* species

Myrna Adianti[1,2], Chie Aoki[1,3], Mari Komoto[1], Lin Deng[1], Ikuo Shoji[1], Tutik Sri Wahyuni[1,2], Maria Inge Lusida[2], Soetjipto[2], Hiroyuki Fuchino[4], Nobuo Kawahara[4] and Hak Hotta[1]

[1]Division of Microbiology, Kobe University Graduate School of Medicine, 7-5-1 Kusunoki-cho, Chuo-ku, Kobe 650-0017, [2]Institute of Tropical Disease, Airlangga University, Jl. Mulyorejo, Surabaya 60115, [3]Japan Science and Technology/Japan International Cooperation Agency Science and Technology Research Partnership for Sustainable Development Laboratory (JST/JICA SATREPS), Faculty of Medicine, University of Indonesia, Jl. Salemba 4, Jakarta 10430, Indonesia and [4]Research Center for Medicinal Plant Resources, National Institute of Biomedical Innovation, 1–2, Hachimandai, Tsukuba City, Ibaraki Prefecture 305-0843, Japan

ABSTRACT

Development of complementary and/or alternative drugs for treatment of hepatitis C virus (HCV) infection is still much needed from clinical and economic points of view. Antiviral substances obtained from medicinal plants are potentially good targets to study. *Glycyrrhiza uralensis* and *G. glabra* have been commonly used in both traditional and modern medicine. In this study, extracts of *G. uralensis* roots and their components were examined for anti-HCV activity using an HCV cell culture system. It was found that a methanol extract of *G. uralensis* roots and its chloroform fraction possess anti-HCV activity with 50%-inhibitory concentrations (IC_{50}) of 20.0 and 8.0 μg/mL, respectively. Through bioactivity-guided purification and structural analysis, glycycoumarin, glycyrin, glycyrol and liquiritigenin were isolated and identified as anti-HCV compounds, their IC_{50} being 8.8, 7.2, 4.6 and 16.4 μg/mL, respectively. However, glycyrrhizin, the major constituent of *G. uralensis*, and its monoammonium salt, showed only marginal anti-HCV activity. It was also found that licochalcone A and glabridin, known to be exclusive constituents of *G. inflata* and *G. glabra*, respectively, did have anti-HCV activity, their IC_{50} being 2.5 and 6.2 μg/mL, respectively. Another chalcone, isoliquiritigenin, also showed anti-HCV activity, with an IC_{50} of 3.7 μg/mL. Time-of-addition analysis revealed that all *Glycyrrhiza*-derived anti-HCV compounds tested in this study act at the post-entry step. In conclusion, the present results suggest that glycycoumarin, glycyrin, glycyrol and liquiritigenin isolated from *G. uralensis*, as well as isoliquiritigenin, licochalcone A and glabridin, would be good candidates for seed compounds to develop antivirals against HCV.

Key words antiviral substance, coumarin, *Glycyrrhiza uralensis*, hepatitis C virus.

Hepatitis C virus is a member of the genus *Hepacivirus* and the family *Flaviviridae*. Based on the heterogeneity of the viral genome, HCV is currently classified into seven genotypes (1–7) and more than 67 subtypes (1a, 1b, 2a, 2b etc.) (1, 2). The viral genome, a single-stranded, positive-sense RNA of 9.6 kb, encodes a polyprotein precursor consisting of about 3000 amino acid residues that is cleaved by host and viral proteases to generate 10 mature proteins, namely core, E1, E2, a putative ion channel p7, and nonstructural proteins NS2, NS3, NS4A, NS4B, NS5A and NS5B (3). Core, E1 and E2 are components of the infectious virus particle together

Correspondence
Hak Hotta, Division of Microbiology, Kobe University Graduate School of Medicine, 7-5-1 Kusunoki-cho, Chuo-ku, Kobe, 650-0017, Japan.
Tel: +81 78 382 5500; fax: +81 78 382 5519. email: hotta@kobe-u.ac.jp

Received 4 December 2013; revised 20 December 2013; accepted 25 December 2013.

List of Abbreviations: CC_{50}, 50%-cytotoxic concentrations; E, envelope; Fr, fraction; GAPDH, glyceraldehyde-3-phosphate dehydrogenase; HCV, hepatitis C virus; IC_{50}, 50%-inhibitory concentration; ID, internal diameter; SI, selectivity index.

with the viral genome; however, the nonstructural proteins constitute the viral replication complex, where replication of the viral genome takes place. The HCV proteins also play essential roles in the pathological processes associated with HCV infection, such as carcinogenesis and glucose and lipid metabolic disorders (4, 5).

Hepatitis C virus is among the major causative agents of chronic hepatitis, hepatic cirrhosis and hepatocellular carcinoma (5–7). The global prevalence of HCV is >2.5%; thus, about 180 million people are chronically infected with this virus worldwide. A variety of standard treatment regimens using combinations of pegylated interferon, ribavirin and other direct-acting agents, such as HCV-specific inhibitors against NS3 protease and NS5A, have been adopted with considerable success. However, some clinically important issues remain unsolved, such as the emergence of drug-resistant virus and the cost of these drugs. Therefore, development of complementary and/or alternative drugs, especially those from medicinal plants, for treating HCV infection is still much needed from both clinical and economic points of view (8, 9).

Glycyrrhiza uralensis and *G. glabra* have been widely used as supplementary treatments in both traditional herbal medicine and modern medicine (10, 11). The radix of *Glycyrrhiza* spp. is commonly known as "gan cao" in Chinese and licorice in English. Bioactive constituents of *Glycyrrhiza* species can be classified into triterpenoids (such as glycyrrhizic acid), coumarins (such as glycycoumarin, glycyrin and glycyrol), flavones (such as liquiritin and liquiritigenin), chalcones (such as isoliquiritigenin and licochalcone A), isoflavans (such as glabridin), stilbenoids and other miscellaneous compounds (11). Glycyrrhizic acid, also known as glycyrrhizin and considered the principal component of *Glycyrrhiza* spp., is a glycosylated triterpenoid saponin that consists of one molecule of glycyrrhetinic acid and two molecules of D-glucuronic acid. Upon hydrolysis, the aglycone, 18β-glycyrrhetinic acid (simply called glycyrrhetinic acid), and two molecules of D-glucuronic acid are released. Glycyrrhizin and other compounds isolated from *Glycyrrhiza* species reportedly have antiviral activity against a variety of viruses, including HIV, herpes simplex virus, influenza virus, severe acute respiratory syndrome coronavirus, hepatitis viruses and enteroviruses (11–15). As for hepatitis viruses, glycyrrhizin has been used to treat liver diseases, including chronic hepatitis B and C (10). Although glycyrrhizin decreases serum alanine aminotransferase concentrations in HCV-infected patients, it does not significantly reduce amounts of HCV RNA (16, 17). It has been reported that a glycyrrhizin-containing preparation reduces hepatic steatosis in transgenic mice expressing the full-length HCV polyprotein (18). Recently, anti-HCV activity of glycyrrhizin *in vitro* was reported (19, 20). However, clear evidence for it still appears to be lacking.

In this study, we used an HCV cell culture system to examine a methanol extract and a chloroform subfraction of *G. uralensis* and certain isolated compounds, as well as commercially available purified compounds, such as glycyrrhizin and glycyrrhetinic acid, for their anti-HCV activity. We report here that glycycoumarin, glycyrin, glycyrol and liquiritigenin isolated from *G. uralensis* showed anti-HCV activity whereas glycyrrhizin showed only a marginal anti-HCV activity. We also found that some other constituents of *G. uralensis* or of *G. inflata* and *G. glabra*, such as isoliquiritigenin, licochalcone A and glabridin, showed anti-HCV activity.

MATERIALS AND METHODS

Cells and viruses

Huh7.5 cells and the plasmid pFL-J6/JFH1 (21) were kindly provided by Dr. C. M. Rice (Rockefeller University, New York, NY, USA). Huh7.5 cells were cultured in Dulbecco's modified Eagle's medium supplemented with FBS (Biowest, Nuaillé, France), non-essential amino acids (Invitrogen, Carlsbad, CA, USA), penicillin (100 IU/mL) and streptomycin (100 μg/mL) (Invitrogen) at 37 °C in a 5% CO_2 incubator. A cell culture-adapted strain of HCV genotype 2a (J6/JFH1-P47) was prepared as described previously (22) and used in this study at an MOI of 2.0.

Extraction, sub-fractionation and purification of *G. uralensis* roots

G. uralensis roots were purchased from Tochimoto Tenkaido (Osaka, Japan). A methanol extract of G. uralensis roots was prepared and subjected to purification procedures, as described previously (23–26). In brief, *G. uralensis* roots were dried at room temperature and pulverized. They were then extracted with methanol at 50 °C for 6 hr. The extracts were filtered and the filtrates concentrated by using an evaporator at temperatures not exceeding 40 °C. The residues obtained were re-suspended in water and successively partitioned between chloroform and *n*-butanol. The chloroform extract was subjected to recycling preparative HPLC (solvent system, 100% methanol; column, GS-320 + GS-310, 21.5 mm ID × 1000 mm, flow rate; 5.0 mL/min; detection, UV 210 nm: Condition A) to afford 10 fractions (Fr.1 to Fr.10). Fr.7 was subjected to HPLC

separation (solvent system, acetonitrile–water; column, Imtakt Unison UK-C18C (Kyoto, Japan), 4.6 mm ID × 250 mm; flow rate, 2.0 mL/min; detection, UV 254 nm) to give 12 fractions (Fr.7–1 to 7–12) and glycyrin (2.5 mg; Fr.7–9). Fr.7–6 was purified by recycling HPLC (Condition A) to afford glycycoumarin (0.7 mg). Fr.8- to Fr.10 were combined and then re-chromatographed by HPLC (solvent system, acetonitrile–water; column, Imtakt Unison UK-C18C, 4.6 mm ID × 250 mm; flow rate, 2.0 mL/min; detection, UV 254 nm) to give 15 fractions (Fr.8–1 to Fr.8–15). Fr.8–3 was subjected to recycling HPLC (Condition A) to give liquiritigenin (1.2 mg). Fr.8–9 was purified by recycling HPLC (Condition A) to afford glycyrol (1.1 mg). The ^{1}H- and ^{13}C-NMR spectra were measured with a Jeol ECA 500 spectrometer (500 MHz; Tokyo, Japan). HPLC was performed on a JASCOLC-2000 plus system (Tokyo, Japan).

Chemicals

Glycyrrhizic acid (cat. no. 074-03481), glycyrrhizic acid mono-ammonium salt *n*-hydrate (cat. no. 075-02171), glycyrrhetinic acid (cat. no. 072-02181) and glabridin (cat. no. 070-04821) were purchased from Wako Pure Chemical Industries (Osaka, Japan). Liquiritin (cat. no. L8045), liquiritigenin (cat. no. 78825) and licochalcone A (cat. no. 68783) were purchased from Sigma–Aldrich (Tokyo, Japan) and isoliquiritigenin (cat. no. I0822) from Tokyo Chemical Industry (Tokyo, Japan). Licorice-saponins G2 (cat. no. P2502) and H2 (cat. no. P2503), and glycyrrhetic acid 3-*O*-glucuronide (cat. no. NH080502) were purchased from Funakoshi (Tokyo, Japan). Glycycoumarin, glycyrol, glycyrin and liquiritigenin were isolated from *G. uralensis* extracts in this study, as described above.

Analysis of anti-HCV activity of plant extracts and purified compounds

Test samples were weighed and dissolved in DMSO to obtain stock solutions at 10 or 30 mg/mL. The stock solutions were stored at −20 °C until used. Huh7.5 cells were seeded in 24-well plates (1.6×10^5 cells/well). HCV was mixed with serial dilutions of the test samples (100, 30, 10, 3 and 1 μg/mL) and inoculated into the cells. After 2 hr, the cells were washed with medium to remove residual virus and further incubated in medium containing the same concentrations of the samples as those during virus inoculation. In time-of-addition experiments, treatment with the samples was performed only during or after virus inoculation in order to assess the mode of action of the samples examined. Culture supernatants were collected 1 and 2 days post-infection and titrated for virus infectivity, as described below. Virus and cells treated with medium containing 0.1% DMSO served as controls. Percent inhibition of the virus infectivity for each dilution of the samples was calculated by comparison with mock-treated controls and IC_{50} determined.

Virus titration

Virus samples were diluted serially 10-fold in complete medium and inoculated onto Huh7.5 cells seeded on glass coverslips in a 24-well plate. After virus adsorption for 2 hr, the cells were washed with medium to remove residual virus and cultured for 24 hr. The virus-infected cells were stained with an indirect immunofluorescence method as reported previously (27). In brief, the virus-infected cells were washed with PBS, fixed with 4% paraformaldehyde for 15 min and permeabilized with 0.1% Triton X-100 in PBS for 15 min at room temperature. After being washed three times with PBS, the cells were incubated with HCV-infected patient's serum for 1 hr, followed by incubation with FITC-conjugated goat anti-human IgG (MBL, Nagoya, Japan). The cells were counterstained with Hoechst 33342 (Molecular Probes, Eugene, OR, USA) for 5 min and HCV-infected cells were counted under a BZ-9000 fluorescence microscope (Keyence, Osaka, Japan).

Cytotoxicity assay

The cytotoxicity of the samples was assessed by WST-1 assay as described previously with a slight modification (27). In brief, Huh7.5 cells in 96-well plates were treated with serial dilutions of the samples or 0.1% DMSO as a control for 48 hr. At the end of the treatment, 10 μL of WST-1 reagent (Roche, Mannheim, Germany) was added to each well and the cells cultured for 1 hr. The WST-1 reagent is absorbed by the cells and converted to formazan by mitochondrial dehydrogenases. The amount of formazan, which correlates with the number of living cells, was determined by measuring the absorbance of each well using a microplate reader at 450 and 630 nm. Percent cell viability compared to the control was calculated for each dilution of the samples and CC_{50} were determined.

Immunoblotting

Cells were lysed with an SDS sample buffer, after which equal amounts of protein were subjected to SDS–polyacrylamide gel electrophoresis and transferred onto a polyvinylidene difluoride membrane (Millipore, Bedford, MA, USA), as described previously (28, 29). The membranes were incubated with the respective primary

antibodies. The primary antibodies used were mouse monoclonal antibodies against HCV NS3 and GAPDH (Millipore). Horseradish peroxidase-conjugated goat anti-mouse immunoglobulin (Invitrogen) was used to visualize the respective proteins by means of an enhanced chemiluminescence detection system (ECL; GE Healthcare, Buckinghamshire, UK).

Real-time quantitative RT-PCR

Real-time quantitative RT-PCR was performed as described previously (28, 29). In brief, total RNA was extracted from the cells using a ReliaPrep RNA cell miniprep system (Promega, Madison, WI, USA) according to the manufacturer's instructions. One microgram of total RNA was reverse transcribed using a GoScript Reverse Transcription system (Promega) with random primers and subjected to real-time quantitative PCR analysis using SYBR Premix Ex Taq (TaKaRa, Kyoto, Japan) in a MicroAmp 96-well reaction plate and an ABI PRISM 7500 system (Applied Biosystems, Foster City, CA, USA). The HCV-specific primers to amplify an NS5A region of the viral genome were 5′-AGACGTATTGAGGTCCATGC-3′ (sense) and 5′-CCGCAGCGACGGTGCTGATAG-3′ (antisense). Human GAPDH gene expression was measured using primers 5′-GCCATCAATGACCCCTTCATT-3′ (sense) and 5′-TCTCGCTCCTGGAAGATGG-3′, which served as an internal control.

RESULTS

Anti-HCV activity of a methanol extract and sub-fractions of *G. uralensis* roots

First, we examined a crude methanol extract of *G. uralensis* roots for anti-HCV activity using the HCV J6/JFH1-P47 strain and Huh7.5 cells. The IC_{50} and CC_{50} values of the crude methanol extract were 20.0 and 300 μg/mL, respectively, the selectivity indexes (SI: CC_{50}/IC_{50}) being 15 (Table 1). We further partitioned the methanol extract using different solvents and found that the anti-HCV activity was concentrated into a chloroform partition, whose IC_{50} and CC_{50} were 8.0 and 93 μg/mL, respectively, the SI being 11.6.

Table 1. Anti-HCV activity (IC_{50}), cytotoxicity (CC_{50}) and selectivity index (SI) of extracts of *G. uralensis* roots

Sample	IC_{50} (μg/mL)	CC_{50} (μg/mL)	SI
Methanol extract	20.0	300	15.0
Chloroform partition	8.0	93	11.6
n-butanol partition	17.5	250	14.3
Water partition	95.0	>500	>5.3

Table 2. Anti-HCV activity (IC_{50}), cytotoxicity (CC_{50}) and selectivity index (SI) of recycling HPLC fractions of chloroform partition of *G. uralensis* roots

Sample	IC_{50} (μg/mL)	CC_{50} (μg/mL)	SI
Fraction 1	>30	>30	na
Fraction 2	>30	>30	na
Fraction 3	>30	>30	na
Fraction 4	>30	>30	na
Fraction 5	20	>30	>1.5
Fraction 6	2.9	65	22
Fraction 7	3.6	40	11
Fraction 8	2.9	40	14
Fraction 9	2.9	>70	>24
Fraction 10	4.9	>70	>14

na, not applicable.

Next, we sub-fractionated the chloroform partition by using recycling HPLC and examined the sub-fractions for anti-HCV activity. We found significant anti-HCV activity with fractions 6–10, IC_{50} ranging between 2.9 and 4.9 μg/mL (Table 2). We further tried to purify a major component(s) in fractions 6–10 by using recycling HPLC: we identified glycycoumarin (30), glycyrin (31), glycyrol (32) and liquiritigenin (33) by NMR spectrum analysis (data not shown).

Anti-HCV activity of *G. uralensis*-derived purified compounds and related chemical compounds obtained from other *Glycyrrhiza* species

We then examined the purified compounds obtained from the *G. uralensis* extracts (glycycoumarin, glycyrin, glycyrol and liquiritigenin) and other *Glycyrrhiza*-derived chemical compounds, such as glycyrrhizin and its derivatives. We found that glycyrrhizin (glycyrrhizic acid) and its monoammonium salt (glycyrrhizic acid monoammonium), the latter being more water-soluble than the former, possessed only marginal anti-HCV activity, IC_{50} values being 180 and 320 μg/mL, respectively (Table 3). The aglycone of glycyrrhizin, glycyrrhetinic acid, showed more significant anti-HCV activity than did glycyrrhizin, its IC_{50} being 40 μg/mL. It should be noted that their anti-HCV activities were weaker than those of the recycling HPLC fractions 6–10 of the *G. uralensis* extract. The monoglucuronide form of glycyrrhizin, glycyrrhetic acid 3-*O*-glucuronide, did not show significant anti-HCV activity at the concentration tested. These results suggest that another compound(s) in fractions 6–10 was responsible for the anti-HCV activity. Two other saponins tested in this study, licorice-saponins G2 and H2, did not show detectable anti-HCV activity. On the other hand, coumarins, such as

Table 3. Anti-HCV activity (IC_{50}), cytotoxicity (CC_{50}) and selectivity index (SI) of *G. uralensis*- and other *Glycyrrhiza* spp-derived compounds

Sample	IC_{50} (μg/mL)	CC_{50} (μg/mL)	SI
Triterpenoids			
Glycyrrhizin	180	560	3.1
Glycyrrhizic acid monoammonium	320	690	2.2
Glycyrrhetic acid 3-O-glucuronide	>30‡	>30	na
Glycyrrhetinic acid	40.0	77.4	1.9
Licorice-saponin G2	>30‡	>30	na
Licorice-saponin H2	>30‡	>30	na
Coumarins			
Glycycoumarin (isolated)	8.8	69.0	7.8
Glycyrin (isolated)	7.2	25.0	3.5
Glycyrol (isolated)	4.6	35.5	7.7
Flavonoids			
Flavanones			
Liquiritin	75.0	570	7.6
Liquiritigenin	16.4	125	7.6
Chalcones			
Isoliquiritigenin	3.7	11.0	3.0
Licochalcone A†	2.5	20.0	8.0
Isoflavan			
Glabridin†	6.2	22.7	3.7

†Not detected in *G. uralensis* (34). ‡No detectable HCV inhibition at 30 μg/mL. na, not applicable.

glycycoumarin, glycyrin and glycyrol, which were isolated in this study (purity >90%) from the *G. uralensis* extracts, showed potent anti-HCV activity, IC_{50} being 4.6–8.8 μg/mL. Liquiritigenin, which was also isolated from the *G. uralensis* extracts, showed weaker anti-HCV activity than the coumarins. Also, isoliquiritigen, licochalcone A and glabridin exhibited potent anti-HCV activity, their IC_{50} being 3.7, 2.5 and 6.2 μg/mL, respectively. It should be noted that licochalcone A and glabridin have been reported to be absent in *G. uralensis* but present in *G. inflata* and *G. glabra* (34).

Mode-of-action of *G. uralensis*-derived isolated compounds and related compounds obtained from other *Glycyrrhiza* species

To determine whether the anti-HCV effects of the compounds of *Glycyrrhiza* species are exerted on the entry or post-entry stage, we performed the following time-of-addition experiments.

1. HCV was mixed with a test compound and the mixture inoculated into the cells. After virus adsorption for 2 hr, the residual virus and test sample were removed and the cells re-fed with fresh medium without the test sample for 46 hr. This experiment examines the antiviral effect at the entry step.
2. HCV was inoculated into the cells in the absence of a test sample. After virus adsorption for 2 hr, the residual virus was removed and the cells treated with the test samples for 46 hr. This experiment examines the antiviral effect at the post-entry step.
3. As a positive control, HCV mixed with the test sample was inoculated into the cells. After virus adsorption for 2 hr, the residual virus and test sample were removed and the cells treated with the test samples for 46 hr.

Table 4. Mode-of-action analysis of anti-HCV activities of *G. uralensis*- and other *Glycyrrhiza* spp.-derived compounds

Compound	Conc. (mg/mL)†	Anti-HCV activity (% inhibition) During‡	After‡	During & after‡
Chloroform partition	30	28.6	100	100
Glycycoumarin	20	16.7	100	100
Glycyrin	15	18.4	98.3	99.6
Glycyrol	10	21.3	100	100
Liquiritigenin	30	15.5	90.0	87.2
Isoliquiritigenin	8	14.1	91.0	82.5
Licochalcone A	5	0	94.4	93.8
Glabridin	12	0	91.0	93.8

†The concentrations of each compound used were 2 × IC_{50}. ‡Treatment with the compound was administered only during, only after or both during and after virus inoculation.

We found that all the *Glycyrrhiza* species-derived compounds as well as the chloroform partition of the *G. uralensis* extract exerted their antiviral effects after virus inoculation (Table 4). These results suggest that all the anti-HCV compounds of *Glycyrrhiza* species tested in this study, namely, glycycoumarin, glycyrin, glycyrol, liquiritigenin, isoliquiritigenin, licochalcone A and glabridin, as well as the chloroform extract, act primarily at the post-entry step.

Inhibition of HCV RNA replication and HCV protein synthesis by glycycoumarin, glycyrin, and glycyrol obtained from *G. uralensis*

To further confirm that *G. uralensis*-derived compounds exert their anti-HCV activities at the post-entry step, Huh7.5 cells were inoculated with HCV for 2 hr, followed by treatment with each of compounds for 1–2 days. The results obtained clearly demonstrated that glycycoumarin, glycyrin and glycyrol inhibit HCV RNA replication, resulting in decreased HCV protein

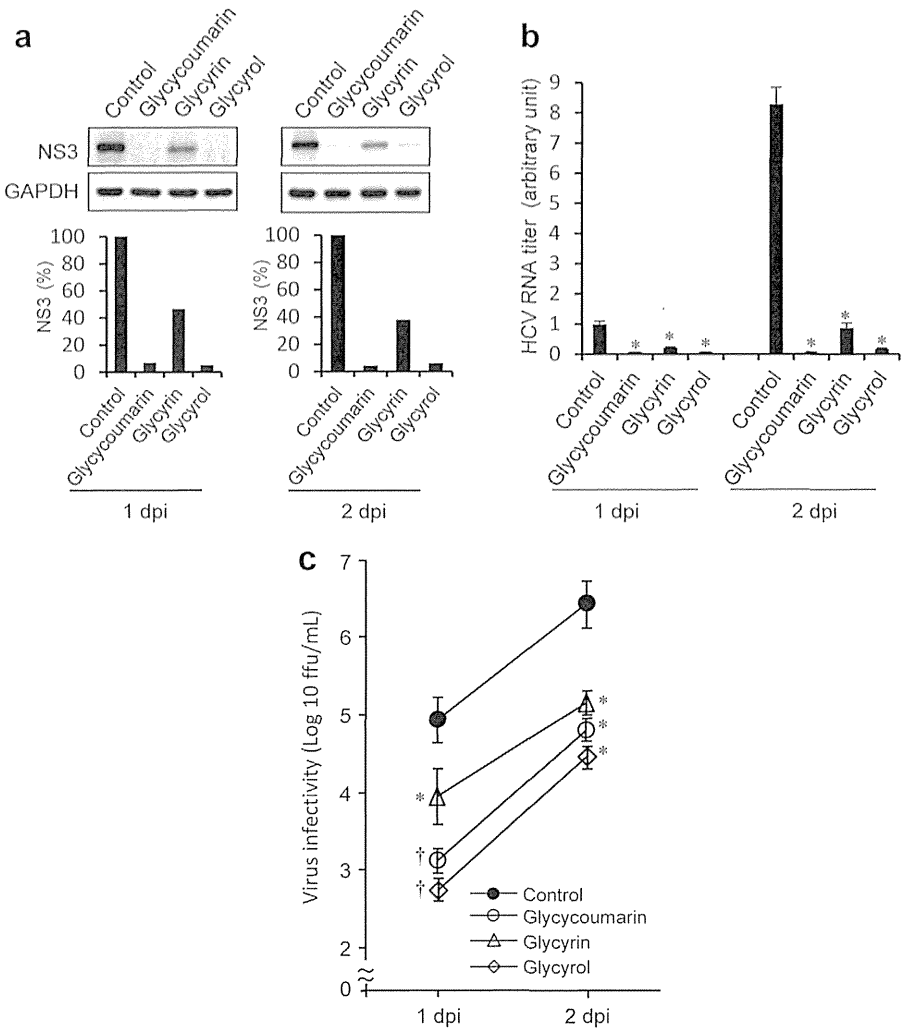

Fig. 1. Effects of glycycoumarin, glycyrin and glycyrol isolated from *G. uralensis* on HCV RNA replication and protein synthesis. (a) Huh 7.5 cells infected with HCV J6/JFH1 and treated with either glycycoumarin (20 μg/mL), glycyrin (15 μg/mL), glycyrol (10 μg/mL) or left untreated were subjected to western blot analysis using monoclonal antibody against the HCV NS3 protein at 1 and 2 days post-infection. GAPDH served as an internal control to verify equal amounts of sample loading. Signal intensities of NS3 were normalized to the corresponding GAPDH signal. (b) Amounts of HCV RNA in the cells described in (a) were measured by real-time quantitative RT-PCR analysis. These amounts were normalized to GAPDH mRNA expression. Data represent means ± SEM of data from two independent experiments. The value for the untreated control at 1 day post-infection is arbitrarily expressed as 1.0. $^{*}P < 0.001$, compared with the control. (c) Amounts of HCV infectious particles in the supernatants of the cultures described in (a) and (b) were determined: data for glycycoumarin, glycyrin, glycyrol and the untreated control are shown. Data represent means ± SEM of data from two independent experiments. $^{*}P < 0.05$; $^{\dagger}P < 0.01$, compared with the untreated control; dpi, days post infection.

synthesis as demonstrated by both real-time quantitative RT-PCR and immunoblotting analyses (Fig. 1a, b). We also confirmed that production of HCV infectious particles is inhibited by glycycoumarin, glycyrin and glycyrol at 1 and 2 days post-infection (Fig 1c).

DISCUSSION

Glycyrrhiza species possess a variety of bioactive compounds, such as: (i) triterpenoids, for example, glycyrrhizin, glycyrrhetic acid 3-*O*-glucuronide, glycyrrhetinic acid and various licorice-saponins; (ii) coumarins, for example, glycycoumarin, glycyrin and glycyrol; (iii) flavanones, for example, liquiritin and liquiritigenin; (iv) chalcones, for example, isoliquiritigenin and licochalcone; (v) isoflavans, for example, glabridin; (vi) stilbenoids, for example, dihydrostilbenes; and other miscellaneous compounds (11). In this connection, flavanones, chalcones and isoflavans are members of flavonoids.

Glycyrrhizin is the major constituent of *Glycyrrhiza* species, representing 1–9% of the total (14). Glycyrrhizin and other compounds isolated from *Glycyrrhiza* species reportedly possess antiviral activity against a variety of viruses (11–15). With regard to HCV, it was recently reported that glycyrrhizin inhibits HCV infection in Huh-7 cells (19, 20). On the other hand, controversial observations have been reported in clinical settings; namely, that glycyrrhizin has no significant effect on amounts of HCV RNA whereas it reduces serum alanine aminotransferase concentrations in HCV-infected patients (16, 17). These apparently contradictory findings might be explained by a membrane-stabilizing effect of glycyrrhizin; clear evidence for antiviral activity of glycyrrhizin is still lacking (10). In the present study, we observed that glycyrrhizin and glycyrrhizic acid monoammonium showed only marginal anti-HCV activity (Table 3). Glycyrrhetinic acid showed significant anti-HCV activity. However, their anti-HCV activities were significantly weaker than that of the HPLC fractions obtained from *G. uralensis* extract. On the other hand, we found that certain coumarins, such as glycycoumarin, glycyrin and glycyrol, and a flavanone, liquiritigenin, isolated from *G. uralensis*, as well as other compounds contained in *Glycyrrhiza* species, possess potent anti-HCV activities. Mode-of-action analysis revealed that all the *Glycyrrhiza*-derived anti-HCV compounds tested act primarily at the post-entry step. Consistent with our observations, other researchers have also reported that two flavonoids, isoliquiritigenin and glycycoumarin, extracted from *Glycyrrhizae radix*, either *G. uralensis* or *G. glabra*, inhibit replication of an HCV subgenomic RNA replicon *in vitro* (35). The IC_{50} values of isoliquiritigenin and glycycoumarin against HCV subgenomic replicon were 6.2 and 15.5 μg/mL, respectively. On the other hand, to the best of our knowledge, there are no published reports so far regarding anti-HCV activities of glycyrin and glycyrol. It has been reported that glycyrin, which is known to possess peroxisome proliferator-activated receptor-γ ligand-binding activity, shows antibacterial activity against *Streptococcus pyogenes*, *Haemophilus influenzae* and *Moraxella catarrhalis* (36–38). Glycyrol reportedly exerts anti-inflammatory effects by binding to calcineurin to inhibit its activity (39, 40). However, the possible antimicrobial activity of glycyrol has not been reported. Further study is needed to elucidate the detailed mechanism of anti-HCV activities of glycyrin and glycyrol, and also possible antiviral activities against viruses other than HCV.

In conclusion, our results suggest that glycycoumarin, glycyrin, glycyrol and liquiritigenin isolated from *G. uralensis*, as well as isoliquiritigenin, licochalcone A and glabridin, would be good candidates for seed compounds to develop antivirals against HCV.

ACKNOWLEDGMENTS

The authors are grateful to Dr. C. M. Rice (Rockefeller University, New York, NY, USA) for providing Huh7.5 cells and pFL-J6/JFH1. This study was supported in part by Science and Technology Research Partnerships for Sustainable Development (SATREPS) from Japan Science and Technology Agency (JST) and Japan International Cooperation Agency (JICA). This study was also carried out as part of the Japan Initiative for Global Research Network on Infectious Diseases (J-GRID), Ministry of Education, Culture, Sports, Science and Technology, Japan.

DISCLOSURE

The authors have no conflicts of interest to declare.

REFERENCES

1. Gottwein J.M., Scheel T.K., Jensen T.B., Lademann J.B., Prentoe J.C., Knudsen M.L., Hoegh A.M., Bukh J. (2009) Development and characterization of hepatitis C virus genotype 1–7 cell culture systems: role of CD81 and scavenger receptor class B type I and effect of antiviral drugs. *Hepatology* **49**: 364–77.
2. Smith D.B., Bukh J., Kuiken C., Muerhoff A.S., Rice C.M., Stapleton J.T., Simmonds P. (2013) Expanded classification of hepatitis C Virus into 7 genotypes and 67 Subtypes: updated criteria and assignment web resource. *Hepatology* **59**: 318–27.
3. Moradpour D., Penin F., Rice C.M. (2007) Replication of hepatitis C virus. *Nat Rev Microbiol* **5**: 453–6.
4. Shoji I., Deng L., Hotta H. (2011) Molecular mechanism of hepatitis C virus-induced glucose metabolic disorders. *Front Microbiol* **2**: 278.
5. Arzumanyan A., Reis H.M., Feitelson M.A. (2013) Pathogenic mechanisms in HBV- and HCV-associated hepatocellular carcinoma. *Nat Rev Cancer* **13**: 123–35.
6. Shepard C.W., Finelli L., Alter M.J. (2005) Global epidemiology of hepatitis C virus infection. *Lancet Infect Dis* **5**: 558–67.
7. Mohd Hanafiah K., Groeger J., Flaxman A.D., Wiersma S.T. (2013) Global epidemiology of hepatitis C virus infection: new estimates of age-specific antibody to HCV seroprevalence. *Hepatology* **57**: 1333–42.
8. Calland N., Dubuisson J., Rouille Y., Seron K. (2012) Hepatitis C virus and natural compounds: a new antiviral approach? *Viruses* **4**: 2197–217.
9. Ploss A., Dubuisson J. (2012) New advances in the molecular biology of hepatitis C virus infection: towards the identification of new treatment targets. *Gut* **61** (Suppl 1): i25–35.
10. Stickel F., Schuppan D. (2007) Herbal medicine in the treatment of liver diseases. *DigLiver Dis* **39**: 293–304.
11. Asl M.N., Hosseinzadeh H. (2008) Review of pharmacological effects of *Glycyrrhiza* sp. and its bioactive compounds. *Phytother Res* **22**: 709–24.

12. Pompei R., Flore O., Marccialis M.A., Pani A., Loddo B. (1979) Glycyrrhizic acid inhibits virus growth and inactivates virus particles. *Nature* **281**: 689–90.
13. Cinatl J., Morgenstern B., Bauer G., Chandra P., Rabenau H., Doerr H.W. (2003) Glycyrrhizin, an active component of liquorice roots, and replication of SARS-associated coronavirus. *Lancet* **361**: 2045–6.
14. Fiore C., Eisenhut M., Krausse R., Ragazzi E., Pellati D., Armanini D., Bielenberg J. (2008) Antiviral effects of Glycyrrhiza species. *Phytother Res* **22**: 141–8.
15. Wang J., Chen X., Wang W., Zhang Y., Yang Z., Jin Y., Ge H.M., Li E., Yang G. (2013) Glycyrrhizic acid as the antiviral component of *Glycyrrhiza uralensis* Fisch. against coxsackievirus A16 and enterovirus 71 of hand foot and mouth disease. *J Ethnopharmacol* **147**: 114–21.
16. van Rossum T.G., Vulto A.G., Hop W.C., Brouwer J.T., Niesters H.G., Schalm S.W. (1999) Intravenous glycyrrhizin for the treatment of chronic hepatitis C: a double-blind, randomized, placebo-controlled phase I/II trial. *J Gastroenterol Hepatol* **14**: 1093–9.
17. Orlent H., Hansen B.E., Willems M., Brouwer J.T., Huber R., Kullak-Ublick G.A., Gerken G., Zeuzem S., Nevens F., Tielemans W.C., Zondervan P.E., Lagging M., Westin J., Schalm S.W. (2006) Biochemical and histological effects of 26 weeks of glycyrrhizin treatment in chronic hepatitis C: a randomized phase II trial. *J Hepatol* **45**: 539–46.
18. Korenaga M., Hidaka I., Nishina S., Sakai A., Shinozaki A., Gondo T., Furutani T., Kawano H., Sakaida I., Hino K. (2011) A glycyrrhizin-containing preparation reduces hepatic steatosis induced by hepatitis C virus protein and iron in mice. *Liver Int* **31**: 552–60.
19. Ashfaq U.A., Masoud M.S., Nawaz Z., Riazuddin S. (2011) Glycyrrhizin as antiviral agent against hepatitis C virus. *J Transl Med* **9**: 112.
20. Matsumoto Y., Matsuura T., Aoyagi H., Matsuda M., Hmwe S.S., Date T., Watanabe N., Watashi K., Suzuki R., Ichinose S., Wake K., Suzuki T., Miyamura T., Wakita T., Aizaki H. (2013) Antiviral activity of glycyrrhizin against hepatitis C virus in vitro. *PLoS ONE* **8**: e68992.
21. Lindenbach B.D., Evans M.J., Syder A.J., Wolk B., Tellinghuisen T.L., Liu C.C., Maruyama T., Hynes R.O., Burton D.R., McKeating J.A., Rice C.M. (2005) Complete replication of hepatitis C virus in cell culture. *Science* **309**: 623–6.
22. Bungyoku Y., Shoji I., Makine T., Adachi T., Hayashida K., Nagano-Fujii M., Ide Y., Deng L., Hotta H. (2009) Efficient production of infectious hepatitis C virus with adaptive mutations in cultured hepatoma cells. *J Gen Virol* **90**: 1681–9.
23. Li S.Y., Fuchino H., Kawahara N., Sekita S., Satake M. (2002) New phenolic constituents from Smilax bracteata. *J Nat Prod* **65**: 262–6.
24. Fuchino H., Sekita S., Mori K., Kawahara N., Satake M., Kiuchi F. (2008) A new leishmanicidal saponin from Brunfelsia grandiflora. *Chem Pharm Bull* **56**: 93–6.
25. Fuchino H., Kawano M., Mori-Yasumoto K., Sekita S., Satake M., Ishikawa T., Kiuchi F., Kawahara N. (2010) *In vitro* leishmanicidal activity of benzophenanthridine alkaloids from *Bocconia pearcei* and related compounds. *Chem Pharm Bull* **58**: 1047–50.
26. Fuchino H., Daikonya A., Kumagai T., Goda Y., Takahashi Y., Kawahara N. (2013) Two new labdane diterpenes from fresh leaves of *Leonurus japonicus* and their degradation during drying. *Chem Pharm Bull* **61**: 497–503.
27. Deng L., Adachi T., Kitayama K., Bungyoku Y., Kitazawa S., Ishido S., Shoji I., Hotta H. (2008) Hepatitis C virus infection induces apoptosis through a Bax-triggered, mitochondrion-mediated, caspase 3-dependent pathway. *J Virol* **82**: 10375–8.
28. Deng L., Shoji I., Ogawa W., Kaneda S., Soga T., Jiang D.P., Ide Y.H., Hotta H. (2011) Hepatitis C virus infection promotes hepatic gluconeogenesis through an NS5A-mediated, FoxO1-dependent pathway. *J Virol* **85**: 8556–68.
29. Wahyuni T.S., Tumewu L., Permanasari A.A., Apriani E., Adianti M., Rahman A., Widyawaruyanti A., Lusida M.I., Fuad A., Soetjipto D., Nasronudin D., Fuchino H., Kawahara N., Shoji I., Deng L., Aoki C., Hotta H. (2013) Antiviral activities of Indonesian medicinal plants in the East Java region against hepatitis C virus. *Virol J* **10**: 259.
30. Demizu S., Kajiyama K., Takahashi K., Hiraga Y., Yamamoto S., Tamura Y., Okada K., Kinoshita T. (1988) Antioxidant and antimicrobial constituents of licorice: isolation and structure elucidation of a new benzofuran derivative. *Chem Pharm Bull* **36**: 3474–9.
31. Kinoshita T., Saitoh T., Shibata S. (1978) A new 3-arylcoumarin from licorice root. *Chem Pharm Bull* **26**: 135–40.
32. Shiozawa T., Urata S., Kinoshita T., Saitoh T. (1989) Revised structures of glycyrol and isoglycyrol, constituents of the root of Glycyrrhiza uralensis. *Chem Pharm Bull* **37**: 2239–40.
33. Chokchaisiri R., Suaisom C., Sriphota S., Chindaduang A., Chuprajob T., Suksamrarn A. (2009) Bioactive flavonoids of the flowers of Butea monosperma. *Chem Pharm Bull* **57**: 428–32.
34. Kondo K., Shiba M., Nakamura R., Morota T., Shoyama Y. (2007) Constituent properties of licorices derived from *Glycyrrhiza uralensis*, *G. glabra*, or *G. inflata* identified by genetic information. *Biol Pharm Bull* **30**: 1271–7.
35. Sekine-Osajima Y., Sakamoto N., Nakagawa M., Itsui Y., Tasaka M., Nishimura-Sakurai Y., Chen C.H., Suda G., Mishima K., Onuki Y., Yamamoto M., Maekawa S., Enomoto N., Kanai T., Tsuchiya K., Watanabe M. (2009) Two flavonoids extracts from *Glycyrrhizae radix* inhibit *in vitro* hepatitis C virus replication. *Hepatol Res* **39**: 60–9.
36. Mae T., Kishida H., Nishiyama T., Tsukagawa M., Konishi E., Kuroda M., Mimaki Y., Sashida Y., Takahashi K., Kawada T., Nakagawa K., Kitahara M. (2003) A licorice ethanolic extract with peroxisome proliferator-activated receptor-gamma ligand-binding activity affects diabetes in KK-Ay mice, abdominal obesity in diet-induced obese C57BL mice and hypertension in spontaneously hypertensive rats. *J Nutr* **133**: 3369–77.
37. Kuroda M., Mimaki Y., Sashida Y., Mae T., Kishida H., Nishiyama T., Tsukagawa M., Konishi E., Takahashi K., Kawada T., Nakagawa K., Kitahara M. (2003) Phenolics with PPAR-gamma ligand-binding activity obtained from licorice (*Glycyrrhiza uralensis* roots) and ameliorative effects of glycyrin on genetically diabetic KK-A(y) mice. *Bioorg Med Chem Lett* **13**: 4267–72.
38. Tanaka Y., Kikuzaki H., Fukuda S., Nakatani N. (2001) Antibacterial compounds of licorice against upper airway respiratory tract pathogens. *J Nutr Sci Vitaminol* **47**: 270–3.
39. Peng L., Qi Y., Wu H., Wei Q. (2011) Interaction of glycyrol with calcineurin A studied by spectroscopic methods and docking. *IUBMB Life* **63**: 14–20.
40. Shin E.M., Zhou H.Y., Guo L.Y., Kim J.A., Lee S.H., Merfort I., Kang S.S., Kim H.S., Kim S., Kim Y.S. (2008) Anti-inflammatory effects of glycyrol isolated from *Glycyrrhiza uralensis* in LPS-stimulated RAW264. 7 macrophages. *Int Immunopharmacol* **8**: 1524–32.

ANTIOXIDANTS & REDOX SIGNALING
Volume 21, Number 1, 2014

DOI: 10.1089/ars.2013.5381

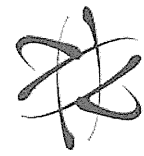

Discoveries

ORIGINAL RESEARCH COMMUNICATION

Nitrosative Stress Induces Peroxiredoxin 1 Ubiquitination During Ischemic Insult *via* E6AP Activation in Endothelial Cells Both *In Vitro* and *In Vivo*

Rong-Rong Tao,[1,*] Huan Wang,[1,*] Ling-Juan Hong,[1] Ji-Yun Huang,[1] Ying-Mei Lu,[2] Mei-Hua Liao,[1] Wei-Feng Ye,[1,3] Nan-Nan Lu,[1] Dan-Yan Zhu,[1] Qian Huang,[4] Kohji Fukunaga,[5] Yi-Jia Lou,[1] Ikuo Shoji,[6] Christopher Stuart Wilcox,[7] En-Yin Lai,[4,7] and Feng Han[1]

Abstract

Aims: Although there is accumulating evidence that increased formation of reactive nitrogen species in cerebral vasculature contributes to the progression of ischemic damage, but the underlying molecular mechanisms remain elusive. Peroxiredoxin 1 (Prx1) can initiate the antioxidant response by scavenging free radicals. Therefore, we tested the hypothesis that Prx1 regulates the susceptibility to nitrosative stress damage during cerebral ischemia *in vitro* and *in vivo*. ***Results:*** Proteomic analysis in endothelial cells revealed that Prx1 was upregulated after stress-related oxygen–glucose deprivation (OGD). Although peroxynitrite upregulated Prx1 rapidly, this was followed by its polyubiquitination within 6 h after OGD mediated by the E3 ubiquitin ligase E6-associated protein (E6AP). OGD colocalized E6AP with nitrotyrosine in endothelial cells. To assess translational relevance *in vivo*, mice were studied after middle cerebral artery occlusion (MCAO). This was accompanied by Prx1 ubiquitination and degradation by the activation of E6AP. Furthermore, brain delivery of a lentiviral vector encoding *Prx1* in mice inhibited blood–brain barrier leakage and neuronal damage significantly following MCAO. ***Innovation and Conclusions:*** Nitrosative stress during ischemic insult activates E6AP E3 ubiquitin ligase that ubiquitinates Prx1 and subsequently worsens cerebral damage. Thus, targeting the Prx1 antioxidant defense pathway may represent a novel treatment strategy for neurovascular protection in stroke. *Antioxid. Redox Signal.* 21, 1–16.

Introduction

BRAIN MICROVASCULAR ENDOTHELIAL CELLS provide a barrier between the bloodstream and brain that is critical in brain development, maturation, and homeostasis (9, 37). The balance between endothelial cell survival and death is pivotal for brain remodeling and repair (41). Increased cell death of cerebrovascular endothelial cells exacerbates inflammatory, ischemic, and degenerative brain diseases (26). Before a new strategy can be developed to counter these adverse effects of ischemia-induced endothelial dysfunction and neurovascular damage, it is necessary to define the factors responsible for ischemia-induced blood–brain barrier (BBB) damage.

Under conditions of intense oxidative stress, such as ischemia or hypoxia injury, increased generation of nitric oxide (NO) and superoxide ($O_2^{\bullet -}$) results in the formation of peroxynitrite ($ONOO^-$) (50). This is a short-lived highly reactive oxidant that attacks and inactivates many proteins. Specifically, $ONOO^-$ irreversibly inactivates prostacyclin

[1]Institute of Pharmacology, Toxicology and Biochemical Pharmaceutics, Zhejiang University, Hangzhou, China.
[2]School of Medicine, Zhejiang University City College, Hangzhou, Zhejiang, China.
[3]The Children's Hospital, Zhejiang University School of Medicine, Hangzhou, China.
[4]Department of Physiology, Zhejiang University School of Medicine, Hangzhou, China.
[5]Department of Pharmacology, Graduate School of Pharmaceutical Sciences, Tohoku University, Sendai, Japan.
[6]Division of Microbiology, Center for Infectious Diseases, Kobe University Graduate School of Medicine, Kobe, Japan.
[7]Hypertension, Kidney, and Vascular Research Center, Georgetown University Medical Center, Washington, District of Columbia.
*Both authors contributed equally to this work.

Innovation

Our study is the first demonstration that nitrosative stress initiates the ubiquitination of peroxiredoxin 1 (Prx1) and subsequent disturbance of redox homeostasis in endothelial cells during ischemia-like injury. Our findings further identified E6-associated protein (E6AP) E3 ligase that ubiquitinated Prx1. Thus, repression of peroxynitrite ($ONOO^-$) formation or *E6AP* knockdown dampened the ischemia-induced disturbance of Prx1 defense signaling. Since an active Prx1 was required for optimal neurovascular cell survival, targeting the Prx1 antioxidant defense pathway may represent a novel treatment strategy for neurovascular protection after stroke.

synthase and oxidizes tetrahydrabiopterin to dihydrabiopterin, thereby uncoupling endothelial NO synthase and directing it to generate $O_2^{\bullet -}$ in place of NO. Indeed, endothelial cells are the primary targets of nitrosative stress in cardiovascular disease, stroke, and neurodegenerative disorders (18, 48). Although nitrosative damage to lipids, proteins, and DNA has been implicated in neurovascular damage following cerebral ischemia, the downstream signaling mechanisms remain elusive (13, 16, 17, 29).

Peroxiredoxins (Prxs) are thiol-specific antioxidant enzymes that maintain redox balance under both normal conditions and oxidative stress (6, 7, 10, 28). Although Prx1 is the most abundant and widely distributed member of the mammalian Prxs (23, 24) and is a recognized peroxide-detoxifying enzyme, its pathophysiological role during brain disease remains unclear (38, 44). Cultured *Prx1*-deficient fibroblasts have decreased proliferation and increased sensitivity to oxidative DNA damage. *Prx1*-deficient mice developed hemolytic anemia caused by increased erythrocytic reactive oxygen species (ROS) (34). Furthermore, mutant Hungtington (*mHtt*) gene expression decreased Prx1 levels and increased its sulfonylation (35).

We tested the hypothesis that Prx1 in endothelial cells in culture and in the brain *in vivo* is a pivotal antioxidant pathway but can be damaged by nitrosative stress during hypoxia or ischemia, thereby exacerbating injury. We report that oxygen/glucose-deprived endothelial cells ubiquitinate Prx1 by nitrosative activation of E3 ubiquitin ligase (E6-associated protein [E6AP]). The outcome is that Prx1 is targeted for degradation leading to cellular redox imbalance and loss of the integrity of the endothelial BBB in mice following ischemia. Repression of $ONOO^-$ formation or *E6AP* knockdown dampened these disturbances of Prx1 defense signaling in endothelial cells. The initial study was made in human umbilical vascular endothelial cells, and key observations were confirmed and extended in human brain microvascular endothelial cells (HBMECs). Thus, our results indicate that Prx1 is a pivotal molecule for the protection of endothelial cells and microvessels from ischemia-induced neurovascular damage both *in vitro* and *in vivo*.

Results

Identification of differentially expressed proteins after oxygen–glucose deprivation in endothelial cells

Two-dimensional gel electrophoresis was performed in EA.hy926 endothelial cells to identify proteins that were differentially expressed between control and oxygen–glucose deprivation (OGD)-treated endothelial cells. Figure 1A shows a silver-stained two-dimensional gel electrophoresis reference map of the OGD-treated endothelial cultures (Fig. 1A, $n=3$, lower) in comparison to the control profile (Fig. 1A, $n=3$, upper). The spots that showed a twofold or greater difference between treatments were further characterized by trypsin digestion and matrix-assisted laser desorption/ionization (MALDI) time-of-flight (TOF) mass spectrometry. Twenty-two different proteins from 36 spots were identified with high confidence (CI % ranging from 97.5% to 100%) (Supplementary Table S1; Supplementary Data are available online at www.liebertpub.com/ars). The identified proteins were classified into functional groups (Supplementary Fig. S1). We selected Prx1 for further study since it was implicated in oxidation–reduction balance and abundantly increased 2.5-fold after OGD treatment (Supplementary Fig. S2A).

Temporal changes of Prx1 protein levels in endothelial cells after OGD

Immunoblotting studies demonstrated a time-dependent increase in Prx1 over 1–6 h followed by a decline after 12 h (Fig. 1B, C). There was a similar pattern of protein levels of heat shock protein 27 (HSP27) (Fig. 1B, C). Molecular chaperones such as HSP27 can defend against protein misfolding after sublethal stressful stimuli (4). Immunocytochemical experiments demonstrated intracellular localization of Prx1 (Fig. 1D), which increased 6 h after OGD treatment in the cytosol of endothelial cells (Fig. 1D, E).

Characterization of OGD-induced Prx1 ubiquitination in endothelial cells

Unexpectedly, our Western blot data demonstrated a continual increase in the density of a broad, high-molecular-weight (>118 kDa) band for Prx1 starting 6 h after OGD treatment (Fig. 2A). A similar increase in a high-molecular-weight band (>118 kDa) was detected following OGD treatment after probing with an anti-ubiquitin antibody (Fig. 2B). The OGD-induced ubiquitination of Prx1 was confirmed and extended in HBMECs (Fig. 3 A, B) and mouse cerebral microvascular endothelial cells (bEnd.3) (Supplementary Fig. S2B).

Inhibition of proteosomal uptake with MG132 or lactacystin also increased the high-molecular-weight isoforms of Prx1 (Fig. 2C and Supplementary Fig. S3). Probing with an anti-Prx1 antibody in ubiquitin immunocomplexes from OGD-treated endothelial cells revealed a predominant band larger than 118 kDa (Fig. 2D and Fig. 3C). OGD-induced ubiquitination of Prx1 was confirmed by the immunoprecipitation of Prx1 followed by immunoblotting with an anti-ubiquitin antibody (Fig. 2E and Fig. 3D). Consistently, Western blot analysis of cell extracts from OGD-treated cells demonstrated that high-molecular-weight conjugates of Prx1 were significantly reduced in *ubiquitin-K48R*-transfected endothelial cells (Fig. 2F and Fig. 3E, F).

The role of Prx1 during proapoptotic cascades after OGD treatment

Proapoptotic proteins were identified by immunoblotting of EA.hy926 cells transfected with either an empty vector or

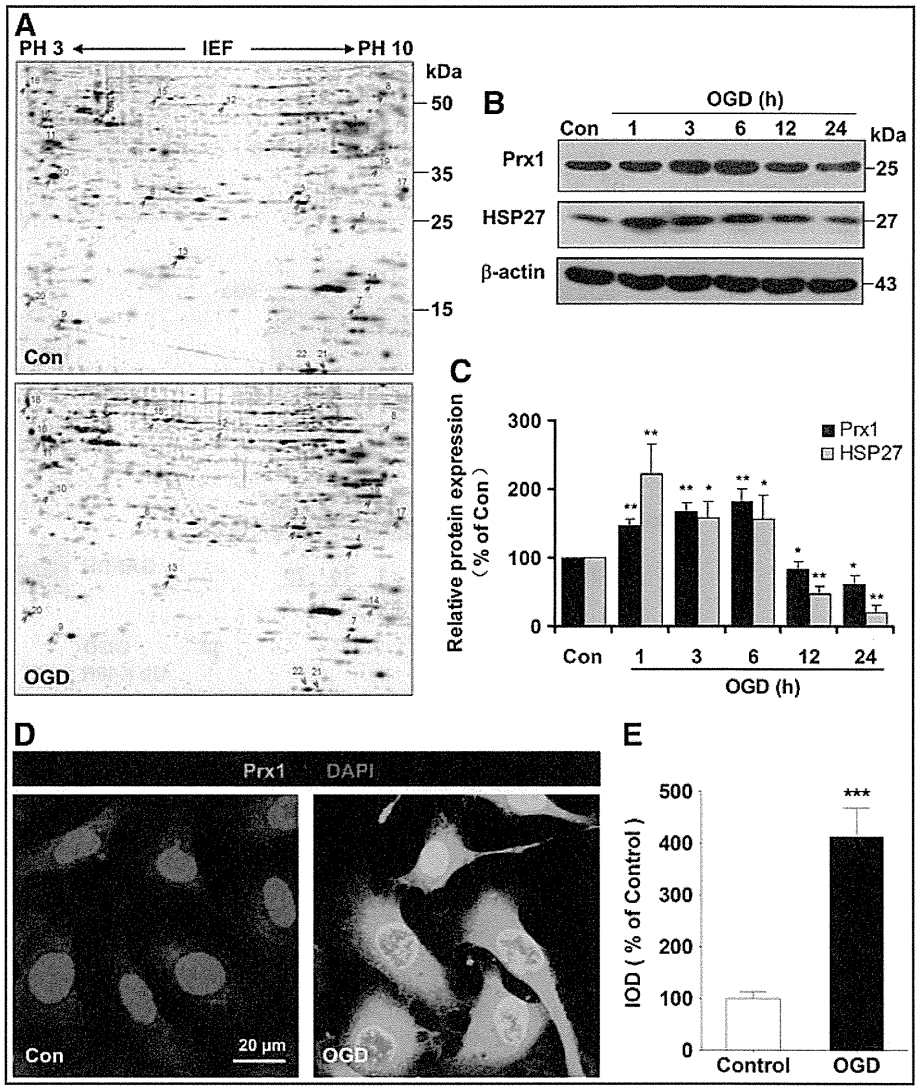

FIG. 1. The proteomic identification of differentially expressed proteins after OGD in endothelial cells. (A) Representative silver-stained two-dimensional gel of control and OGD-treated EA.hy926 endothelial cells. Whole proteins (450 μg) were separated on a non-linear pH gradient (3–10) followed by 12% SDS-PAGE. **(B)** Time course of Prx1 and HSP27 protein levels in cell lysates of endothelial cells following OGD. Quantifications of the temporal changes of Prx1 and HSP27 protein levels are shown in **(C)**. Immunoblots are representative of three independent experiments. $*p<0.05$; $**p<0.01$ *versus* control. Immunoblotting with an anti-β-actin antibody showed equal amounts of loaded protein in each lane. **(D)** Changes in the immunostaining of Prx1 (green) 6 h after OGD. Subcellular localization of Prx1 was determined by laser confocal microscopy. Data are representative of three independent experiments. Scale bar = 20 μm. **(E)** Quantification of Prx1 immunofluorescence expressed as IOD as described in the Materials and Methods section. $***p<0.001$ *versus* control. IOD, integrated optical density; HSP27, heat shock protein 27; OGD, oxygen–glucose deprivation; Prx1, peroxiredoxin 1; SDS-PAGE, sodium dodecyl sulfate–polyacrylamide gel electrophoresis. To see this illustration in color, the reader is referred to the web version of this article at www.liebertpub.com/ars

a *Prx1* expression vector following OGD insult (Fig. 4). Calnexin is a type I integral endoplasmic reticulum (ER) membrane chaperone involved in folding newly synthesized (glycol) proteins (8). Overexpression of Prx1 significantly inhibited calnexin, PERK, and Ire-1α degradation (Fig. 4A, B) and also inhibited caspase-3 and poly ADP-ribose polymerase (PARP) cleavage (Fig. 4C, D). Exposure of vector-transfected cells to OGD for 6 h decreased the phosphorylation of anti-apoptotic proteins, such as phospho-ERK (Thr202/Tyr204) and phospho-FKHR (Ser256) (forkhead transcription factor Foxo1), and also decreased the protein levels of heme oxygenase-1 (HO-1) but increased the phosphorylation of c-Jun N-terminal kinase (JNK) and P38 (Fig. 4E, F). By contrast, overexpression of *Prx1* after OGD injury resulted in significant upregulation of anti-apoptotic proteins in endothelial cells (Fig. 4E, F). Exposure of vector-transfected cells to OGD for 6 h elevated terminal deoxynucleotidyl transferase dUTP nick end labeling (TUNEL)-positive staining (Fig. 4G, H), whereas overexpression of Prx1 effectively decreased TUNEL staining (Fig. 4G, H). The apoptosis of endothelial cells was determined using flow cytometry with Annexin V-FITC/propidium iodide (PI). In contrast to control cells (2.20%), we found that OGD treatment induced elevation in the fraction of Annexin V/PI-positive cells (49.92%). Moreover, *Prx1* small interfering RNA (siRNA) transduction further exaggerated OGD-induced cell death (Fig. 4I). The present data demonstrate that Prx1 elicits an anti-apoptotic effect after OGD injury in endothelial cells, coinciding with its antioxidant function in the endothelium (31).

E6AP activation contributes to Prx1 stress response after OGD

Since Prx1 has been identified as a novel E6AP-binding protein (33), the present study further elaborates the role of E6AP in ubiquitination of Prx1 during OGD. Representative blots are presented in Figure 5A and show that E6AP was activated following OGD exposure over 1–24 h (Fig. 5A). Similar change of E6AP was confirmed in HBMEC (Supplementary Fig. S4A, B) and bEnd.3 endothelial cells after OGD (Supplementary Fig. S2B). Immunocytochemical analysis of the endothelial cells revealed OGD-induced strong immunoreactivity for E6AP (red fluorescence) that was undetectable in control cells (Fig. 5B–D and Supplementary Fig. S4C, D), which suggests that OGD-induced ubiquitination of Prx1 is associated with E6AP activation.

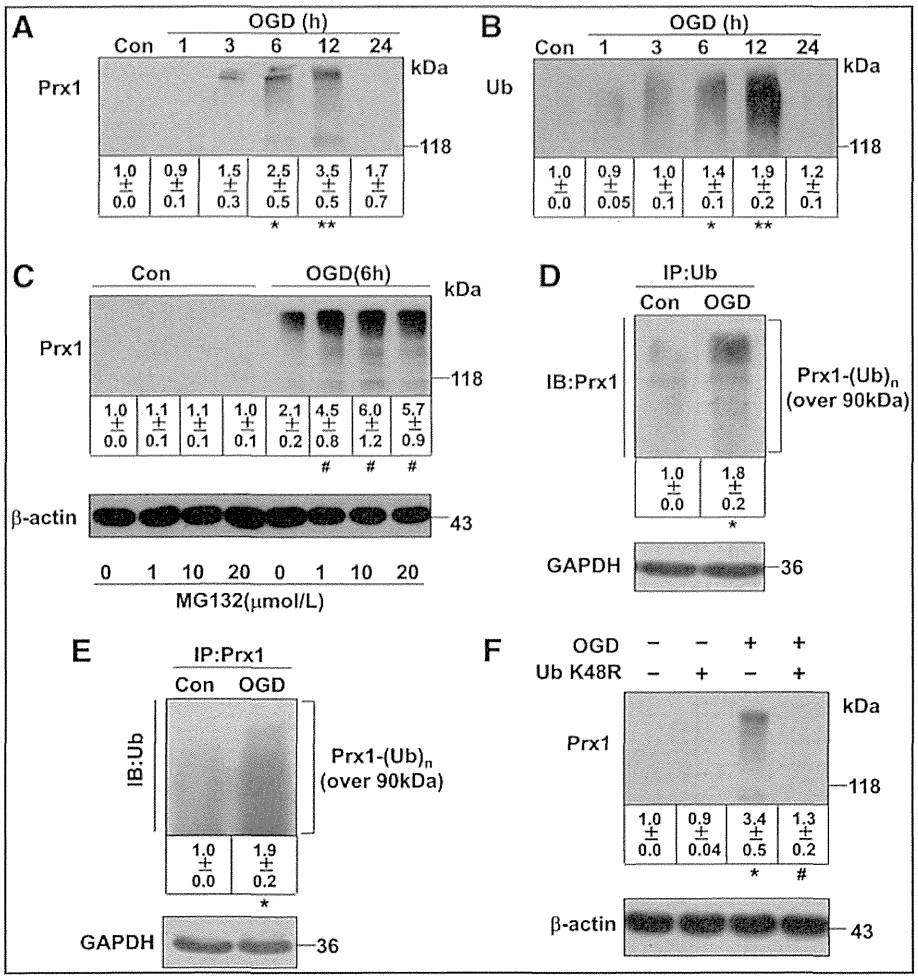

FIG. 2. OGD induces ubiquitination of Prx1 in EA.hy926 endothelial cells. **(A)** Temporal changes in the high-molecular-weight Prx1 isoform were observed in OGD-treated endothelial cells. The accumulated polyubiquitinylated proteins were detected by Western blot analysis with anti-Prx1 antibody. **(B)** Protein ubiquitination status after OGD treatment in endothelial cells. The accumulated multiubiquitinylated proteins were detected by Western blot analysis with an anti-ubiquitin antibody. **(C)** The changes in polyubiquitinated Prx1 were detected following OGD treatment of endothelial cells with or without proteasome inhibitors. The endothelial cells were treated with 1, 10, or 20 μM MG132 or DMSO 30 min before OGD. The cells were then washed, harvested after 6 h OGD, and analyzed for polyubiquitinated Prx1 levels. **(D)** The OGD-induced ubiquitination of Prx1 was detected by the immunoprecipitation of ubiquitin followed by immunoblotting with an anti-Prx1 antibody. **(E)** Immunoprecipitation of Prx1 from cell lysates of OGD-treated endothelial cells followed by blotting with an anti-ubiquitin antibody. **(F)** The ubiquitin K48R mutant decreased OGD-induced Prx1 ubiquitination in endothelial cells. Endothelial cells were cultured and transfected with plasmid DNA encoding the *ubiquitin-K48R* mutant or an empty plasmid, followed by OGD and immunobloting analysis. Immunoblots are representative of three independent experiments. Data are expressed as the percentage of values of control (mean ± SEM). $^{*}p < 0.05$; $^{**}p < 0.01$ *versus* control; $^{\#}p < 0.05$ *versus* OGD.

E6AP and the active-site cysteine-to-alanine-inactivated mutant E6AP were expressed in mammalian *p3869HA-E6AP C-A* cells (22, 46). Here, after 48 h of transfection, siRNA knockdown of *E6AP* (Fig. 5E, F) or transfection with the *E6AP C-A* mutant (Fig. 5G, H) both significantly blunted the ubiquitination of Prx1 in OGD-treated endothelial cells.

Nitrosative stress associated with the Prx1 defensive response after OGD

The $ONOO^-$ donor 3-morpholinosydnonimine (SIN-1) induced early dose-dependent elevation of Prx1 (Supplementary Fig. S5A, B) and Prx1 ubiquitination (Fig. 6A, B) in endothelial cells as detected by immunoblot, accompanied by increased Prx1 immunostaining (Fig. 6C) and activation of E6AP (Fig. 6D). Whereas increased nitrotyrosine immunostaining and E6AP immunoreactivity were observed in OGD-treated cells (Fig. 6E, F), inhibition of $ONOO^-$ with uric acid markedly reduced both nitrotyrosine and E6AP immunostaining after OGD exposure (Fig. 6E). This was confirmed by Western blot (Fig. 6G, H). A similar result was observed in endothelial cells treated with $ONOO^-$ decomposition catalysts (FeTPPS, 1 μM) (Supplementary Fig. S6A, B). E6AP immunoprecipitates from the cell lysates were probed with anti-nitrotyrosine antibody (Fig. 6I). The results

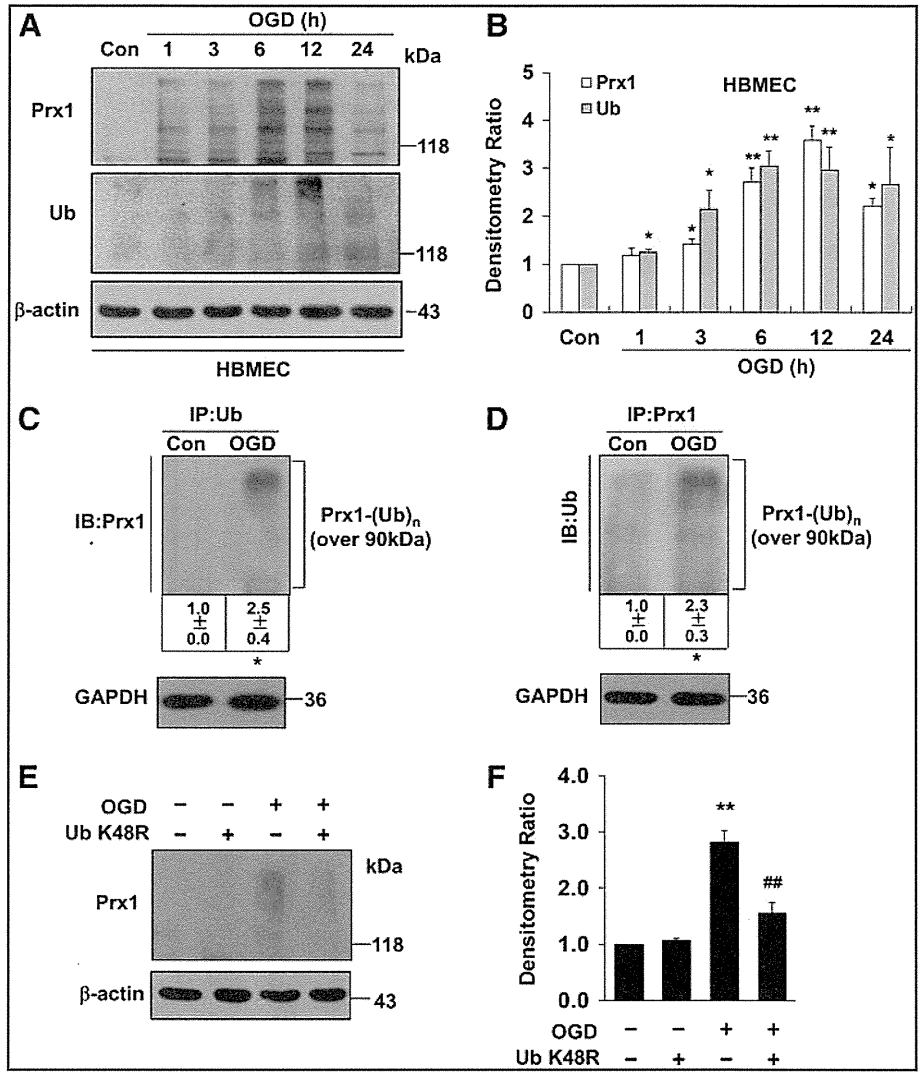

FIG. 3. The ubiquitination of Prx1 in OGD-treated HBMEC. **(A)** The time-dependent change of OGD-induced Prx1 and ubiquitin expression in HBMECs was detected by Western blot. **(B)** Densitometry of the Western blots for **(A)** was normalized by the level of β-actin as an internal control. **(C)** OGD-treated HBMEC endothelial cells were lysed and subjected to immunoprecipitation with antibodies to ubiquitin. The resultant precipitates were then subjected to immunoblot analysis with antibodies to Prx1. **(D)** Immunoprecipitation of Prx1 from lysed HBMEC with or without OGD treatment were collected for immunoblot analysis with ubiquitin antibody. **(E)** The *ubiquitin-K48R* mutant transfection attenuates Prx1 ubiquitination in OGD-treated endothelial cells. HBMEC were cultured and transfected with plasmid DNA encoding the *ubiquitin-K48R* mutant or an empty plasmid. **(F)** Densitometry of the Western blots for **(E)** was normalized by the level of β-actin as an internal control. Immunoblots are representative of three independent experiments. Data are expressed as the percentage of values of control (mean ± SEM). $^{*}p<0.05$; $^{**}p<0.01$ *versus* control; $^{\#\#}p<0.01$ *versus* OGD. HBMEC, human brain microvascular endothelial cell.

demonstrated that the E6AP/nitrotyrosine interaction in OGD-treated endothelial cells was significantly increased. Consistently, OGD-induced tyrosine nitration of E6AP was further confirmed by the immunoprecipitation of nitrotyrosine followed by immunoblotting with an anti-E6AP antibody (Fig. 6J). In addition, Prx1 immunoprecipitates from the lysates were probed with anti-nitrotyrosine antibody demonstrating that OGD did not induce Prx1 protein co-immunoprecipitate with nitrotyrosine (Supplementary Fig. S7). Melatonin blunted the ubiquitination of Prx1 in OGD-treated cells (Supplementary Fig. S8), suggesting that nitrosative stress induced Prx1 ubiquitination during OGD.

E6AP activation contributes to Prx1 stress response in brain microvessels after transient middle cerebral artery occlusion in mice

Since there are limited *in vivo* data on the degradation of Prx1 by ubiquitin ligases in ischemic brain, we used a mouse transient middle cerebral artery occlusion (tMCAO) model for further study. The immunoreactivity for E6AP was observed predominantly in the ipsilateral brain microvessel endothelium 6 h after tMCAO (Fig. 7A-e), accompanied by increased Prx1 immunoreactivity (Fig. 7A-d). A representative Z-stack image is shown in Figure 7B. However, after 24 h, Prx1 was downregulated where E6AP remained upregulated in the brain microvessel endothelium (Fig. 7A, g-i). Ubiquitination of Prx1 was elevated significantly in the brain microvessels 6 h after MCAO (Fig. 7C, D), whereas Prx1 staining was observed in microvessels of sham-operated animals where ubiquitin staining was absent. To further determine E6AP as a key modulator in nitrosative stress-mediated cerebrovascular damage *in vivo*, we stereotaxically delivered a lentivirus carrying mouse sh*E6AP* into the ventricle in mice 2 weeks before MCAO, followed by ischemia and 24 h reperfusion. Western blot analysis showed that lentivirus-mediated cerebral *E6AP* knockdown reduced cerebrovascular damage, which was demonstrated by preventing ischemia-induced dephosphorylation of prosurvival kinases and tight junction proteins breakdown (Fig. 7E–G).

Lentiviral-Prx1 brain transduction protects against neurovascular damage in tMCAO mice

Two weeks after the cerebroventricular injection of a lentiviral-GFP vector encoding mouse *Prx1* (LV-*Prx1*), there was efficient and sustained GFP fluorescence in the brain ventricles (Fig. 8A), cortex (Fig. 8B), hippocampus, and

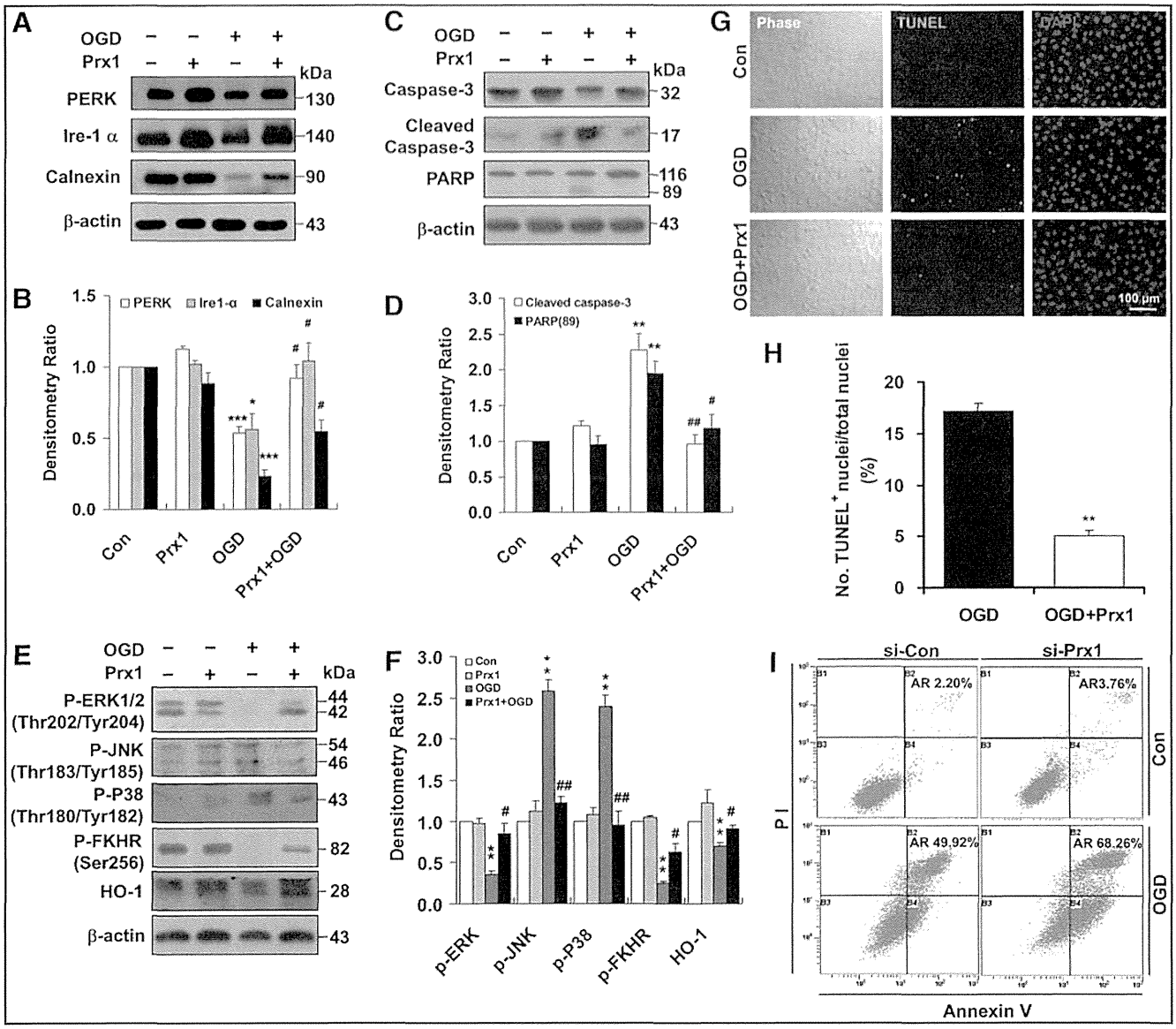

FIG. 4. Role of Prx1 in the OGD-induced apoptotic cascade in endothelial cells. (**A**) The effects of Prx1 on OGD-induced ER stress signaling were determined by immunoblotting. (**B**) Densitometry of Western blots for PERK, Ire-1α, and calnexin levels 6 h after OGD, with or without *Prx1* transfection. Data are expressed as densitometry ratio of control (mean ± SEM). $*p < 0.05$; $***p < 0.001$ *versus* control; $^{\#}p < 0.05$ *versus* OGD. (**C**) The effects of Prx1 overexpression on OGD-induced caspase-3 and PARP levels were evaluated by immunoblotting. EA.hy926 cells were cultured and transfected with plasmid DNA encoding *Prx1* or an empty plasmid using Attractene. (**D**) The quantification data for blots are shown in (**C**). Data are expressed as densitometry ratio of control (mean ± SEM). $**p < 0.01$ *versus* control; $^{\#}p < 0.05$; $^{\#\#}p < 0.01$ *versus* OGD. (**E**) The effects of Prx1 overexpression on OGD-induced protein levels were evaluated by immunoblotting. Cells were transfected with *Prx1* plasmid followed by 6 h of OGD or control stimulation. Cell lysates were prepared and resolved by SDS-PAGE. The proteins were immunoblotted with antibodies against phospho-ERK, phospho-JNK, phospho-P38, phospho-FKHR (Ser256), and HO-1. (**F**) Quantitative analysis of protein levels for (**E**) was performed by densitometry. Data are expressed as densitometry ratio of control (mean ± SEM). $**p < 0.01$ *versus* control; $^{\#}p < 0.05$; $^{\#\#}p < 0.01$ *versus* OGD. (**G**) Changes in apoptosis 6 h after OGD were detected using the TUNEL assay. Double staining was performed for TUNEL (green) and DAPI (blue). The representative images show the increased percentage of TUNEL-positive apoptotic endothelial nuclei (green fluorescence) 6 h after OGD. Scale bar = 100 μm. (**H**) Quantification of TUNEL-positive apoptotic endothelial cells with or without *Prx1* transfection. Apoptosis was dramatically reduced following the overexpression of the *Prx1* gene in endothelial cells after OGD. $**p < 0.01$ *versus* OGD group. (**I**) Representative flow cytometric dot plots of apoptotic cells after OGD with or without *Prx1*siRNA transfection. Cultured EA.hy926 cells were stimulated for 6 h with OGD with or without *Prx1*siRNA transfection. Cells were double-stained with Annexin-V and PI and analyzed by FACS. Immunoblots are representative of three independent experiments. β-Actin was used as the loading control. DAPI, 4′,6-diamidino-2-phenylindole; ER, endoplasmic reticulum; HO-1, heme oxygenase-1; JNK, c-Jun N-terminal kinase; PARP, poly ADP-ribose polymerase; siRNA, small interfering RNA; TUNEL, terminal deoxynucleotidyl transferase dUTP nick end labeling; PI, propidium iodide. To see this illustration in color, the reader is referred to the web version of this article at www.liebertpub.com/ars